USING MEASUREMENTS AND FLOW MODELS TO ASSESS STORMWATER INTERACTIONS IN WOODCHIP PILES

By

MATTHEW THOMAS AMATO

A thesis submitted to the

School of Graduate Studies

Rutgers, The State University of New Jersey

In partial fulfillment of the requirements

For the degree of

Master of Science

Graduate Program in Environmental Sciences

Written under the direction of

Daniel Giménez

And approved by

_____

_____

_____

New Brunswick, New Jersey

[October, 2019]

ABSTRACT OF THE THESIS

USING MEASUREMENTS AND FLOW MODELS TO ASSESS STORMWATER INTERACTIONS IN WOODCHIP PILES

By

MATTHEW THOMAS AMATO

Thesis Director:

Daniel Giménez

Storing woodchips in outdoor piles can have potentially deleterious environmental impacts, including risks from fire and pollution of nearby water resources. Thus, being able to predict leachate quantities and monitor water content within woodchip piles would be advantageous for assessing risk, as well as for developing stormwater management practices for wood recycling operations to follow.

In the first part of this thesis, the leachate generated from three experimental piles (~30 m^3) of woodchips ground either once or twice was continuously collected over a period of six months. Transient three-dimensional flow through the experimental piles was simulated using the numerical model HYDRUS 3D in order to quantify leachate generation. The Bayesian Markov Chain Monte Carlo algorithm $DREAM_{ZS}$ was used to optimize hydraulic flow parameters for a single porosity (SPM) and dual porosity (DPM) model to predict leachate generation based on the water retention and hydraulic conductivity characteristics of the woodchip materials. Model performance statistics verified that both models adequately predicted 6-hour leachate volumes (Nash-Sutcliffe efficiency index: >0.7; Root mean square error: <27 liters per 6-hr), although the

DPM was prone to numerical difficulties. The models are most suitable for predicting leachate produced by storm events with less than 1 cm of rainfall in 6-hr. During more intense rainfalls, leachate generation was systematically under predicted on average by about 20%. This information is important for designing leachate collection and control systems based on different design storm criteria. Additionally, the size and the geometry of the woodchip pile along with the initial moisture content of the woodchips are also likely to influence leachate generation.

Direct knowledge of the water content within woodchip piles is useful for avoiding fire hazards and simulating leachate generation. A reflectometry method was used for estimating volumetric water content (θ) in woodchips taking into consideration their particle size distribution (PSD), temperature (T) and the dielectric permittivity of the dry woodchips plus air. The bulk dielectric permittivity of fine, medium and coarse PSDs were measured from dry to saturated water contents with CS616-L reflectometers at approximately 10°, 24°, 37°, 55° and 70° C. Calibration equations were developed using a multivariate power law function fitted to the data with a hierarchical Bayesian inference procedure. As θ and T increased and PSD became coarser the fitted relationships became more uncertain. Overall the method was most accurate for taking measurements in partially saturated fine woodchip mixtures with median particle diameters smaller than 4 mm and at temperatures between 10° C to 37° C.

Building on the topics explored in this thesis, future research is necessary to engineer an optimal woodchip pile configuration that minimizes the risk of fire and reduces how much leachate can be potentially generated. This information is crucial both from a policy- and practice-based viewpoint.

Acknowledgements

To my family, friends and mentors, I would not have made it this far without your love, your lessons and your support. I am especially appreciative to:

My advisor, Dr. Daniel Giménez, for his devoted guidance and assistance, and also for teaching me the value of hard work.

My committee members, Drs. Peter F. Strom and Uta Krogmann, for believing in me and for their invaluable contributions to my thesis.

My former adviser, Dr. Zofia Gagnon, for always putting her students first and for getting me involved in research.

The New Jersey Department of Environmental Protection for providing the funding that made this research possible.

My brother, Josh, for being my foundation, my motivation and my best friend. I am grateful to have you by my side.

And most importantly, my parents, Ralph and Leslie, for raising me *exactly* the way you did – with endless love and unwavering support. You will always be my role models.

Table of Contents

Abstract ... ii

Acknowledgements ... iv

List of Tables ... vii

List of Figures ... viii

List of Symbols ... xi

1. **Introduction** ... 1
    - **1.1 References** ... 4
2. **Forecasting Leachate Generation from Piles of Ground Woody Biomass using a Three-Dimensional Transient Flow Model** ... 8
    - **2.1 Abstract** ... 8
    - **2.2 Introduction** ... 9
    - **2.3 Flow Theory** ... 12
    - **2.4 Materials & Methods** ... 14
        - *2.4.1 Field Experiment* ... 14
        - *2.4.2 Model Setup* ... 16
        - *2.4.3 Model Optimization* ... 18
        - *2.4.4 Posterior Analysis* ... 20
        - *2.4.5 Model Performance and Validation* ... 21
    - **2.5 Results & Discussion** ... 22
        - *2.5.1 Parameter Estimability* ... 23
        - *2.5.2 Parameter Inference* ... 25
        - *2.5.3 Model Performance* ... 26
        - *2.5.4 Future Improvements* ... 28
    - **2.6 Conclusions** ... 29
    - **2.7 References** ... 30
3. **Dielectric Permittivity-Water Content Relationships in Woodchips: Particle Size and Temperature Effects** ... 47
    - **3.1 Abstract** ... 47
    - **3.2 Introduction** ... 48
    - **3.3 Materials & Methods** ... 50
        - *3.3.1 Experiment* ... 51

3.3.2 Determination of the Water Content **53**

3.3.3 Apparent Bulk Dielectric Permittivity **54**

3.3.4 Inference **55**

3.3.5 Calibration **57**

3.3.6 Validation **58**

3.4 Results & Discussion **59**

3.4.1 Particle Size and Temperature Effects **60**

3.4.2 Calibration **63**

3.4.3 Validation **64**

3.5 Conclusions **65**

3.6 References **66**

4. Future Work **80**

Appendices **81**

Appendix A. Preliminary analysis of the relationship between pile configuration and leachate generation **82**

List of Tables

Table 2.1 Setup for the SPM and DPM inferences with DREAM$_{ZS}$. The prior distributions $p(x)$ are given in the notation $N(\mu, \sigma)$, which stands for a univariate normal distribution with mean μ and standard deviation σ. The min and max of the Range column represent the bounds on each parameter's possible proposal space **35**

Table 2.2 Summary of measurements. The parameters below the dashed line are the fitting parameters in Eq. 7 used to describe the woodchip particle size distributions **36**

Table 2.3 Estimability rankings for six combinations of SPM and DPM parameters from Subroy *et al.* (2014) **37**

Table 2.4 The *maximum a posteriori* (MAP) estimates and mean ± standard deviation of the posterior distributions (Dist.) of the optimized SPM and DPM water retention parameters for the L1 and R2 piles **38**

Table 2.5 Goodness-of-fit statistics (mean ± standard deviation) for the SPM and DPM models using 100 random posterior samples using all data (All) or a subset that excluded the unexpected measured responses (UR) when significant storms occurred, but no leachate was measured (Fig. 2.2). The R2 optimized parameters for the SPM and DPM were validated in the F2 woodchip pile..... **39**

Table 3.1 Summary of functions that describe the $\theta \; vs \; \varepsilon_b$ relationship in various wood materials. The I.D. refers to its curve displayed in Figure 3.4 ..... **70**

Table 3.2 Means (standard deviations) of the effective volumes (cm^3) for the CS616-L sensors during wetting (Saturating) and gravity-driven drainage (Draining) of mixtures of predominantly fine, medium and coarse particle sizes **71**

Table 3.3 Summary of the replicate $\sqrt{\varepsilon_{sa}}$ values for the fine, medium and coarse woodchip mixtures and their parameter's posterior distribution (n=40,000 samples) (Eq. 5) given as the mean (standard deviation). The posterior parameter estimates in "All" were derived after pooling the data from the three particle size groups (Eq. 6). The root mean square error ($RMSE$) was inferred simultaneously with the calibration parameters and the coefficient of determination (R^2) was calculated by evaluating the goodness-of-fit of the 40,000 samples in the posterior distribution **72**

List of Figures

Figure 1.1 Timeline of how the United States has managed municipal wood waste from 1960 to 2015 (Modified from USEPA, 2018) **5**

Figure 1.2 Pictures of the two most common pile configurations used to store woodchips **6**

Figure 1.3 Conceptual diagram along with news headlines highlighting the potential environmental impacts of storing woodchips in outdoor stockpiles **7**

Figure 2.1 (A) Diagram of the experimental setup and leachate collection system. (B) A picture of the experimental setup. (C) A discretized three-dimensional HYDRUS domain based on the L1 pile geometry. The arrows show how precipitation (P) and evaporation (E) fluxes occur from the topmost surfaces, while leachate (L) fluxes leave by a seepage face designated as the bottom surface of the swale **40**

Figure 2.2 Cumulative leachate volumes collected from the three experimental piles compared to measurements of hourly precipitation from the Mansfield, NJ weather station **41**

Figure 2.3 Results of subtracting the posterior distributions of the twice ground woodchip pile R2 from the once ground woodchip pile L1 (contrast=L1-R2). The result of each parameter contrast is a density distribution (shaded in color) with an IQR denoted by the dashed vertical lines. The solid line indicates the position of a contrast equal to zero **42**

Figure 2.4 Correlation scatter plots and density distributions (shaded in color) for the hydraulic parameters of the DPM model after combining the posterior distributions for the L1 and R2 piles. The normal distribution indicated by the solid line represents that parameter's prior probability distribution (Table 2.1). The dashed and solid lines on the x-axis represent the *maximum a posteriori* (MAP) parameter estimates for the L1 and R2 piles, respectively (Table 2.4). The straight lines drawn through the scatter plots are the best fit line and the titles are the parameter's correlation/covariance **43**

Figure 2.5 Cumulative measured leachate volume compared with the 95% interval of confidence predicted by the SPM and DPM water retention models (not including the storms with lacks of leachate responses- Fig. 2.2). The 2.5^{th} and 97.5^{th} percentiles were calculated based on the simulation results of N=100 posterior samples. To predict leachate from the F2 pile, the posterior for the R2 hydraulic parameter sets (Table 2.4) were used **44**

Figure 2.6 HYDRUS predictions from the R2 optimizations (N=100) versus measurements of 6-hr leachate for the F2 woodchip pile. The vertical lines denote the interval between the minimum and maximum leachate prediction. The solid black line represents a perfect 1:1 correlation, while SPM-Cor and DPM-Cor are the best fit linear correlation for each water retention model **45**

Figure 2.7 Analysis of residuals (predictions minus measurements) broken down into small (Sm; green), medium (Med; blue) and large (Lrg; red) 6-hr storm events **46**

Figure 3.1 Particle size distributions for the three types of woodchip samples used in the calibration experiments. The dashed lines represent fits with the functions shown. Modified from Subroy *et al.* (2014). **73**

Figure 3.2 Illustration of the experimental setup. Measurements from the water content reflectometer (CS616-L) and thermistor (109-L) were collected with a data logger (CR1000). Readings from the balances were stored directly in the computer **74**

Figure 3.3 Changes in the output of the CS616-L sensor with respect to the distance of the water level from the waveguide (positioned at Y=0 cm). Measurements were taken while the containers were filled with deionized water and the waveguides were embedded in either the fine mix, coarse mix (Fig. 3.1), or in air. The two-dimensional ellipse (not drawn to scale) depicts the A-A' cross-sectional view of the hypothetical three-dimensional half-ellipsoid effective volume for the coarse woodchip mixture. The three shaded areas represent progressive filling of the container at three times (t) and the associated effect on the sensor's response due to partial filling of the effective volume..... **75**

Figure 3.4 Relationships of A.) $\theta \ vs \ \varepsilon_b$ and B.) $\theta \ vs \ \sqrt{\varepsilon_b}$ taken from published functions (see Table 3.1) that have been used for various kinds of woody material. The shaded area represents the observed range of measurements made in this study. Each curve spans the θ interval used in its development..... **76**

Figure 3.5 Empirical distributions of the values after contrasting the posterior distributions of the group-level parameters (α, β) of Eq. 4 for A.) particle size and B.) temperature groups. The 95% credible interval for the parameter contrasts are contained within the shaded region of the distribution. The vertical dashed line indicates a contrast equal to 0. Subscripts on the α and β parameters denote which particle size or temperature groups are being compared **77**

Figure 3.6 Measurements of $\sqrt{\varepsilon_b}$ for mixtures of predominantly fine, medium and coarse particle sizes made at different temperatures within water content ranges of A.) 0.2-0.25

cm^3/cm^3, B.) 0.4-0.45 cm^3/cm^3 and C.) 0.6-0.65 cm^3/cm^3. The central line represents the median, the ends of the box represent the lower and upper quartiles, the whiskers represent 2.698 standard deviations above and below the median and the symbols are potential outliers..... **78**

Figure 3.7 Results of using the posterior distribution for the particle size-specific parameters of Eq. 5 (see Table 3.3). The data are measurements from saturating/draining laboratory experiments (Lab S/D), laboratory validation measurements determined with the gravimetric method (Lab Static) and the field validation measurements from the experimental stockpile (Field). The 95% P.I. interval for θ (*i.e.,* calculated from the posterior estimates of the $RMSE$) is represented by the wider band and the 95% Cr.I. for θ (*i.e.,* calculated from the posterior estimates of the inferred parameters) is represented by the narrower band..... **79**

List of Symbols

Symbol	Description	Example of Dimension
Symbols in flow models		
θ	Volumetric water content	$m^3\ m^{-3}$
R	Rainfall	$m^3\ hr^{-1}$
E	Evaporation	$m^3\ hr^{-1}$
L	Leachate	$m^3\ hr^{-1}$
h	Pressure head	
K	Hydraulic conductivity	$m\ hr^{-1}$
θ_r	Residual volumetric water content	$m^3\ m^{-3}$
θ_s	Saturated volumetric water content	$m^3\ m^{-3}$
α, m, n	Fitting parameters in the van Genuchten (1980) model	
K_s	Saturated hydraulic conductivity	$m\ hr^{-1}$
S_e	Effective volumetric water content ($S_e = \frac{\theta(h)-\theta_r}{\theta_s-\theta_r}$)	
w_1, w_2	Dual pore partitioning parameter in the Durner (1994) model	
$\alpha_1, m_1, n_1,$ $\alpha_2, m_2, n_2,$	Fitting parameters for the dual pore systems in the Durner (1994) model	
Symbols in estimability analysis		
$\hat{Y}$	Simulated volumetric leachate generation per 6 hours	$m^3\ 6\text{-}hr^{-1}$
p_k	Value of the kth hydraulic parameter under evaluation	
$I_{t,k}$	Sensitivity coefficient for the kth hydraulic parameter at each time step t	
Z	Sensitivity matrix with $t\ x\ k$ dimensions	
Symbols describing goodness-of-fit		
E_f	Nash and Sutcliffe (1970) efficiency index	
$\bar{\bar{Y}}$	Average of the 6-hour leachate measurements	$m^3\ 6\text{-}hr^{-1}$

$RMSE$	Root mean square error	m^3 6-hr^{-1}, m^3 m^{-3}
$RMSD$	Root mean square deviation	m^3 m^{-3}
bias	Percent bias; average residual divided by the average measurement	
Symbols in Bayesian inference		
$p(x\|Y)$	Posterior probability distribution	
$L(Y\|x)$	Likelihood function	
$p(x)$	Prior probability distribution	
$\hat{R}$	Scale reduction statistic to diagnose MCMC convergence (Gelman and Rubin, 1992)	
Symbols to describe woodchip mixtures		
d	Particle diameter	µm
d_{50}	Median particle diameter	µm
d_g	Geometric mean particle diameter	µm
I_d, k_d	Fitting parameters describing the particle size distribution	
ρ_d	Dry bulk density	Mg m^{-3}
θ_{init}	initial volumetric moisture content	m^3 m^{-3}
Symbols that describe dielectric properties		
ε_b	Apparent bulk dielectric permittivity	
ε_s	Dielectric permittivity of oven dry wood material	
ε_w	Dielectric permittivity of water	
P	Period output of the CS616-L water content reflectometer	sec
f_r	Pulse reflections per second	sec^{-1}
S_f	Scaling factor for the CS616 reflectometer model	
t_d	Time delay between the step pulse voltages emitted by the reflectometer	sec
c	Speed of light	m sec^{-1}
L_a	Apparent length of the CS616-L waveguide	cm

$\sqrt{\varepsilon_{sa}}$	Square root of the dielectric permittivity of the dry wood material plus air	
T	Temperature	°C

1. Introduction

Wood waste that is chemically untreated and unpainted, such as pallets, crates and the woody components of yard waste is often recycled into woodchip products that can be used as mulch, composting bulking agent or animal bedding. Determining the fractional amount of wood waste that is recycled and processed into woodchips in the United States is challenging; although the increasing trend of municipal wood recycling (Fig. 1.1) suggests that woodchip production might also be increasing (Falk and McKeever, 2004; USEPA, 2018).

The processing and management of woodchip materials varies by state and recycling facility. Typically, wood recycling facilities grind incoming materials either once into a coarse mixture of woodchips or twice into a fine mixture. The processed woodchips are then stored in outdoor piles up to 20 feet high that are conical or windrow shaped (Fig. 1.2). Woodchips managed in open stockpiles are an environmental risk due to their ability to catch on fire, as well as pollute nearby water resources (Fig. 1.3).

Heat that is generated from biodegradation processes occurring within woodchip piles causes them to undergo self-heating. If the internal temperature of the woodchip piles rises to about 80° C these biodegradation processes virtually cease. However, abiotic degradation processes may then takeover that can cause the pile's internal temperature to continue increasing, possibly until combustion occurs. Thus, to prevent fire hazards, it is imperative to keep woodchip piles well-aerated and sufficiently moist (Buggeln and Rynk, 2002).

Issues of water pollution start with the rain and sprinkler water that percolates through woodchip piles, which solubilizes and transports the organic compounds released by the decomposing wood. Water can exit the pile via evaporation processes, but a substantial portion will flow through the

pile and eventually seep out from its base. This water is referred to as leachate and its quantity/quality likely depends on the intensity of the wetting event, the characteristics of the woodchips and the stockpile management strategy (Tao *et al.,* 2005; Hedmark and Scholz, 2008; Bedane *et al.,* 2011; Svensson *et al.,* 2014; King *et al.,* 2014).

In July of 1999, runoff from two New Jersey (NJ) Class B wood recycling facilities was linked to separate incidents of aquatic eco-system pollution (NJDEP, 2009). Runoff generated from the first facility was being discharged into a nearby lake, which over time depleted its oxygen concentration, and caused a fish kill and an outbreak of avian botulism. At the second facility, a filamentous bacterium known as "sewage fungus" (*Sphaerotilus*) was found growing in a stream where the runoff from one of their woodchip piles was being discharged.

These and other incidents around the state prompted the New Jersey Department of Environmental Protection (NJDEP) to take action under the New Jersey Pollutant Discharge Elimination System regulations (N.J.A.C. 7:14A). In order to make an informed policy decision, NJDEP sponsored Rutgers University to investigate the potential environmental hazards associated with mismanaged runoff from wood recycling operations.

The leachate/combined runoff collected from controlled experimental woodchip piles and several NJ Class B facilities was found to have low pH, relatively low loads of nutrients and a high oxygen demand comparable to raw sewage (Kannepalli, 2014). These findings were provided to NJDEP along with the guidance that the leachate/combined runoff from wood recycling operations should not be released directly into the environment off-site. This in turn motivated a further investigation to determine how stormwater runoff at wood recycling facilities should be managed. The research that is included in this thesis has two separate scientific objectives: (1) to optimize an unsaturated flow model

that can be used to quantify leachate generation from woodchip piles; and (2) to calibrate an automatable reflectometer probe for measuring water content within woodchip piles.

In previous related work, the water retention and unsaturated hydraulic conductivity for different woodchip particle size mixtures were characterized (Subroy, 2013) and a controlled field experiment was carried out in which the leachate from three experimental piles was continuously collected over a period of six months (Kannepalli, 2014). Chapter II of this thesis discusses the hydraulic properties of woodchips and how they can be used to simulate transient leachate generation. Three-dimensional unsaturated flow through the experimental piles was numerically simulated and subsets of hydraulic parameters were inferred based on their ability to simulate the time series measurements of leachate. The optimized hydraulic models are utilizable as a forecasting tool to estimate leachate generation based on woodchip pile size and shape.

Chapter III assesses the applicability of using a reflectometry method to monitor water content in bulk woodchip mixtures. A relationship between bulk dielectric permittivity and volumetric water content in the woodchips was calibrated by considering the effects of particle size distribution, temperature and porosity. The findings in Chapters II and III are intended to help wood recycling managers to be able to monitor and to predict potential leachate generation, as well as to retrofit the necessary stormwater infrastructure to control it. Understanding how to measure water content and forecast flow through woodchips is also relevant to practitioners in the agricultural, energy, and forestry industries.

1.1 References

Bedane, A. H., Afzal, M. T., Sokhansanj, S., 2011. Simulation of temperature and moisture changes during storage of woody biomass owing to weather variability. *Biomas Bioenergy. 35*(7), 3147-3151.

Buggeln, R., Rynk, R., 2002. Self-Heating In Yard Trimmings: Conditions Leading To Spontaneous Combustion. *Compost Sci Util*, 10(2), 162-182.

Falk, R.H., McKeever, D.B., 2004. Recovering wood for reuse and recycling: a United States perspective, in: European COST E31 Conference-Management of Recovered Wood: Recycling, Bioenergy and Other Options. University Studio Press, Thessaloniki, Greece, pp. 29–40.

Hedmark, A., Scholz, M., 2008. Review of environmental effects and treatment of runoff from storage and handling of wood. *Bioresour. Technol.* 99(14), 5997-6009

Kannepalli, S., 2014. *Environmental issues in organics recycling: Reed bed biosolids reuse and leachate from wood mulch stockpiles*. (*Doctoral Dissertation*), Rutgers, The State University of New Jersey, New Brunswick, New Jersey

King, M., Macdonald, G., Hutchinson, M., Seekings, B., 2014. A comparison of the quantity and quality of leachate generated by five compost feedstocks exposed to simulated rainfall. *J. Solid Waste Technol. Manage. 40*(1), 57-69.

New Jersey Department of Environmental Protection, 2009. Bureau of nonpoint pollution control. New Jersey pollutant discharge elimination system. Fact sheet. (R7) General permit for wood recycling facilities. http://www.nj.gov/dep/dwq/pdf/r7_final_permit.pdf.

Subroy, V., 2013. *Hydraulic properties of recycled wood material. (M.S. Thesis)*, Rutgers, The State University of New Jersey, New Brunswick, New Jersey

Svensson, H., Marques, M., Kaczala, F., Hogland, W., 2013. Leaching patterns from wood of different tree species and environmental implications related to wood storage areas. *Water Environ. J. 28*(2), 277-284.

Tao, W., Hall, K.J., Masbough, A., Frankowski, K., Duff, S.J., 2005. Characterization of leachate from a woodwaste pile. *Water Qual. Res. J. Can.* 40, 476–483.

United States, New Jersey Department of Environmental Protection. (1993). *New Jersey pollutant discharge elimination system/discharge to surface water (NJPDES/DSW) permit NJ0005622*. Trenton, NJ: Dept. of Environmental Protection and Energy, Wastewater Facilities Regulation Program, Bureau of Standard Permitting.

USEPA, 2018. *Advancing Sustainable Materials Management: 2015 Fact Sheet*. Washington, DC: U.S. Environmental Protection Agency, Office of Land and Emergency Management.

Figure 1.1 Timeline of how the United States has managed municipal wood waste from 1960 to 2015 (Modified from USEPA, 2018).

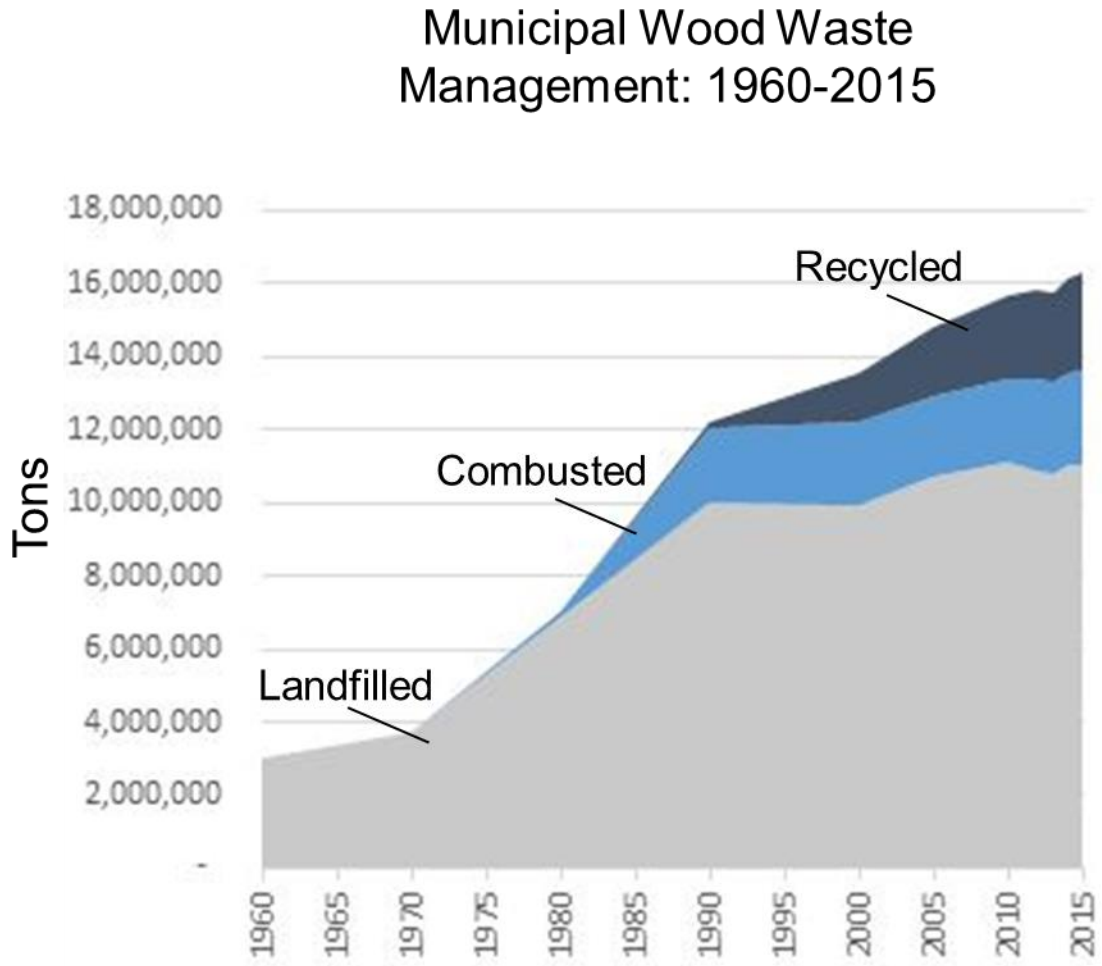

Figure 1.2 Pictures of the two most common pile configurations used to store woodchips.

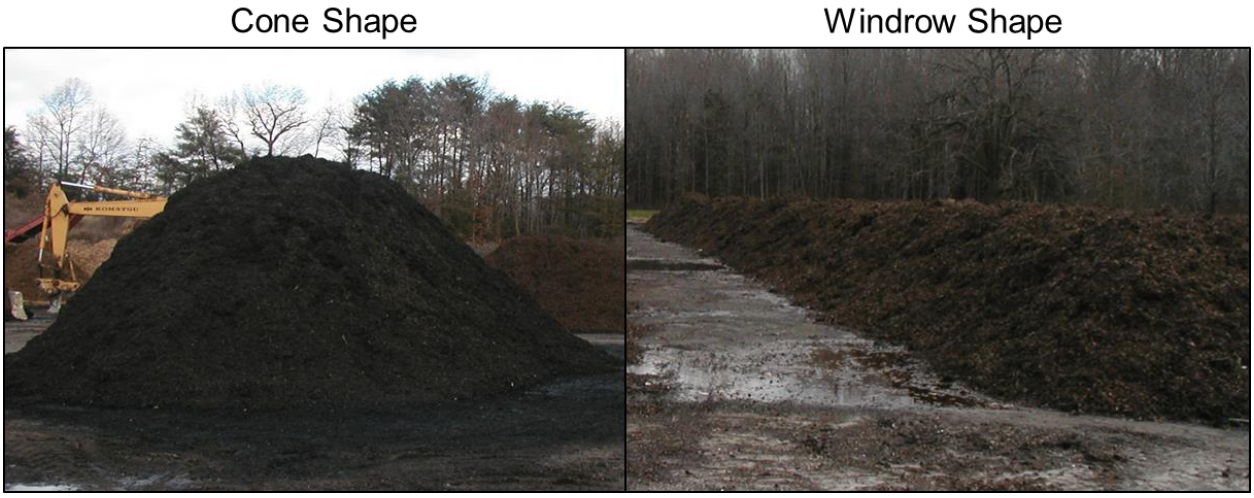

Figure 1.3 Conceptual diagram along with news headlines highlighting the potential environmental impacts of storing woodchips in outdoor stockpiles.

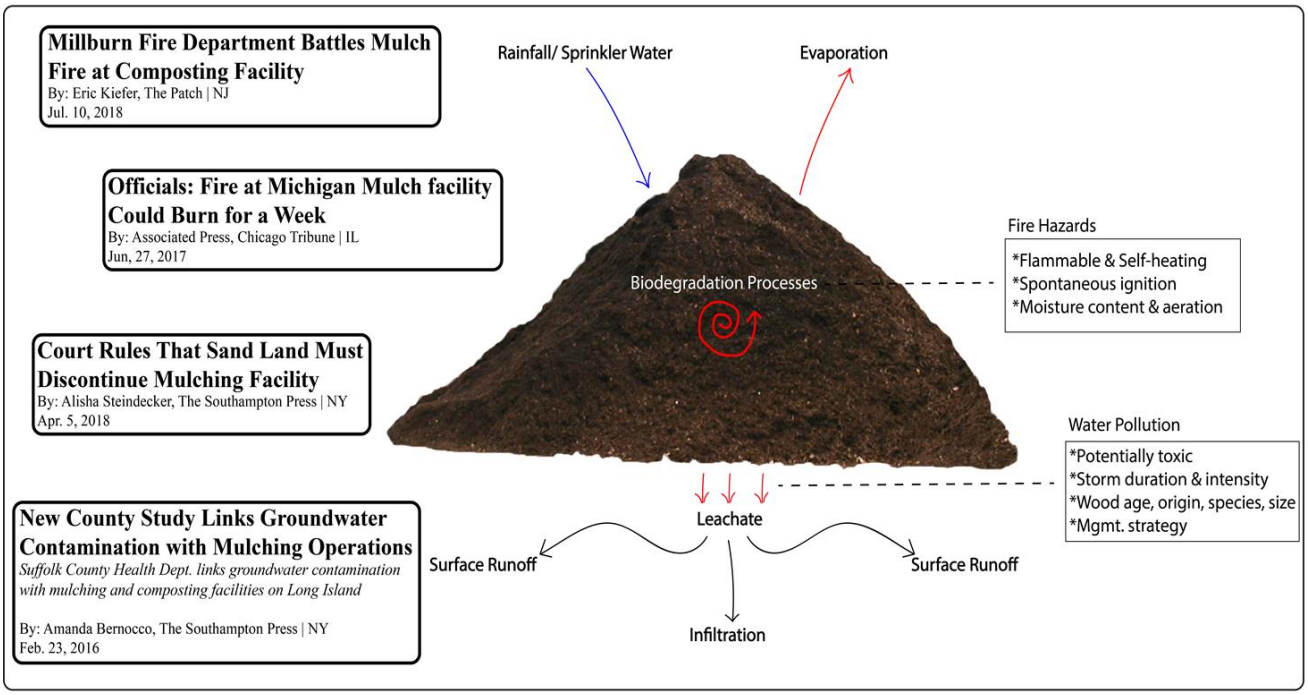

2. Forecasting Leachate Generation from Woodchip Stockpiles using a Three-Dimensional Transient Flow Model

2.1 Abstract

Leachate from open stockpiles of recycled woodchip materials is potentially harmful to aquatic ecosystems. Information about the hydraulic properties of woodchips can be used to simulate transient flow through stockpiles, although these properties must be validated with experiments prior to using them to predict leachate generation at the field-scale. In this study, the leachate from each of three experimental piles of once and twice ground woodchips with approximate volumes of 30 m^3 and median particle lengths of approximately 1 and 2.5 mm, was continuously collected over a period of six months. The numerical model HYDRUS 3D was used in conjunction with the Bayesian MCMC algorithm $DREAM_{ZS}$ to optimize a subset of three or four parameters of hydraulic models that assume either a single porosity (SPM) or dual porosity (DPM) system, respectively. A sensitivity analysis showed that total porosity and the parameter defining the steepness of the water retention relationship were ranked most influential for simulating leachate, while saturated hydraulic conductivity was consistently ranked one of the least. The optimized distributions of parameters for the two woodchip sizes were not significantly different from each other, thus they were combined and summarized with a multivariate Gaussian distribution due to apparent parameter interdependencies. Sampling from the multivariate distribution of DPM parameters reduced how often the model crashed from 23% to 5%. Nash-Sutcliffe efficiency indexes for the optimized models were always above 0.6. Although during intense (more than 1 cm in 6-hr) rainfall events, leachate was under predicted by 13-27%. The optimized models can be used as a tool for developing best management guidelines by examining how different management strategies influence the quantity and quality of leachate.

2.2 Introduction

An estimated 36 million metric tons of municipal wood and woody yard wastes are generated annually in the United States and of that approximately 20% is recovered for reuse (Falk and McKeever, 2004; USEPA, 2018). Recycling facilities processing untreated and unpainted wood into woodchip products grind the incoming wood once or twice, and store the woodchips outdoors in stockpiles for weeks up to several months before use (SWANA, 2002). Stockpiling woodchips is also common in the pulp, agricultural, forestry and energy industries, although management practices differ depending on the intended use of the woodchips (Afzal *et al.,* 2009; Lenz *et al.,* 2015; Lin and Pan, 2015; Hofmann *et al.,* 2017).

Open stockpiles of recycled woodchip materials that are mismanaged can have several adverse environmental impacts, including risks from fires (Li *et al.,* 2006) and contamination of nearby water resources (Kannepalli *et al.,* 2016). Rain and sprinkler water that percolates through the bulk medium solubilizes, suspends and transports organic components released by the decomposing wood. Water that is not retained within the woodchip pile either evaporates or leaches from the stockpile's base where it can infiltrate into the ground or contribute to surface runoff.

Leachate generated from recycled woodchip stockpiles can have a low pH and a high oxygen demand and may contain toxic wood degradation compounds, all of which make it potentially harmful to aquatic ecosystems (Kannepalli *et al.,* 2016). The quality and quantity of this leachate is influenced by the duration and intensity of the wetting event, the characteristics of the wood materials (*e.g.*, age, origin, species and particle size), and stockpile management, including the type of surface it is kept on, pile size and shape, and whether or not the piles are covered (Tao *et al.,* 2005; Hedmark and Scholz, 2008; Bedane *et al.,* 2011; Svensson *et al.,* 2014; King *et al.,* 2014). The quantity of leachate can be predicted with transfer models and hydrograph-based techniques, similar to the prediction of runoff for

designing stormwater control infrastructure at open waste storage facilities (Tollner and Das, 2004; Wilson *et al.,* 2004; Kalaba *et al.,* 2007; Duncan *et al.,* 2013). However, such models often neglect or simplify the hydrological processes occurring within the stockpiled material itself, rendering it difficult to analyze or predict leachate generation- the primary contributor to pollutant loads.

Numerical models are better suited for simulating transient flow through woodchip piles as they implement concepts of mass conservation to approximate the movement of water in space and time (Ferrero *et al.,* 2009; Zambra *et al.,* 2011; Bedane *et al.,* 2011; Seng *et al.,* 2012). HYDRUS (PC-Progress, Prague, CZ) is an established numerical modeling software package for simulating multi-dimensional flow in unsaturated permeable media (Simunek *et al.,* 2012). In the past, HYDRUS has been used to design leachate control measures for conceptual 2D systems of stockpiled mining waste rock and landfilled solid waste (Molson *et al.,* 2005; Fala *et al.,* 2005; Khire and Mukherjee, 2007; Safari *et al.,* 2012; Namaghi *et al.,* 2015). It has also been used to assess the performance of woodchip bioreactors in 1D field-scale tracer studies (Jaynes *et al.,* 2016). In this study, flow was simulated in three-dimensions through cone-shaped pile systems based on the geometries of actual experimental woodchip piles in an effort to predict leachate generation.

Simulating transient flow with HYDRUS requires information about the hydraulic properties of the bulk material, which is in large part influenced by the particle size distribution and the geometry of the pore network (Han *et al.,* 2011; Jaynes *et al.,* 2016). Unsaturated hydraulic properties for different woodchip particle size mixtures were recently inferred from HYDRUS 1D inverse simulations of laboratory multi-step outflow experiments (Subroy *et al.*, 2014). These authors reported that flow through woodchips was best simulated when the pore network was modeled as two interacting pore size distributions (bimodal) representing the inter- and intra-particle pore networks that exist in the bulk mixtures. However, for finely graded woodchip mixtures that had geometric mean particle diameters

below ~4 mm, outflow was adequately predicted using a water retention model based on a single pore size distribution (unimodal).

The optimized water retention parameters based on unimodal and bimodal assumptions still require validation in a field experiment before using them to more broadly forecast leachate generation. Furthermore, it is likely that the flow parameters derived from one dimensional experiments will require additional optimization if they are extrapolated for use in a three-dimensional system (Laloy *et al.*, 2010). This highlights the importance of validating the accuracy of using HYDRUS 3D to predict leachate generation with experimental data from field-scale woodchip piles.

Bayesian inference using Markov Chain Monte Carlo (MCMC) techniques is a global optimization strategy that uses Bayes theorem to update the prior probabilities of unknown model parameters in light of new experimental evidence (Gelman *et al.,* 2015). However, for modeling nonlinear processes such as unsaturated water movement in three-dimensions, a prohibitively large number of MCMC samples may be required to efficiently explore the posterior parameter spaces (Vrugt, 2016). Consequently, MCMC can be inefficient for calibrating CPU-demanding forward models without adjusting the optimization strategy, such as reducing the number of parameters subjected to inference or using informative prior distributions (Scharnagl *et al.,* 2011).

Estimability analyses quantify the identifiability of each unknown model parameter based on its individual influence over predicting specific model outputs (McLean and McAuley, 2012). The orthogonalization method as described by Yao *et al.* (2003) ranks unknown model parameters based on their local sensitivity and correlation structure. This technique has recently been used to determine which parameters of a unimodal water retention model can be uniquely inferred with respect to specific space-time variables, such as outflow measured from a field lysimeter (Ngo *et al.*, 2013; 2014).

The objective of this work was to numerically simulate three-dimensional unsaturated flow using HYDRUS 3D, in order to predict leachate generation from field-scale woodchip piles. Three experimental piles comprised of two different woodchip particle size mixtures were setup outdoors and the leachate they generated, as well as local meteorological conditions, were recorded continuously over a period of six months. Unimodal and bimodal pore models implemented in HYDRUS 3D were applied to simulate transient flow through the experimental piles and a subset of parameters from each pore model, selected with the method of Yao *et al.,* (2003), were optimized using a Bayesian MCMC inference procedure (Vrugt, 2016).

2.3 Flow Theory

The HYDRUS modeling software (HYDRUS 2D/3D, PC-Progress, Prague, CZ) was used to simulate isotropic flow dynamics through rigid permeable media using a modified version of Richards' equation (Simunek *et al.,* 2012)

$$\frac{\partial \theta}{\partial t} = \frac{\partial}{\partial x}\left[K\left(\frac{\partial h}{\partial x}\right)\right] + \frac{\partial}{\partial y}\left[K\left(\frac{\partial h}{\partial y}\right)\right] + \frac{\partial}{\partial z}\left[K\left(\frac{\partial h}{\partial z}\right) + 1\right] + R - E - L \quad (1)$$

where θ ($m^3\ m^{-3}$) represents volumetric water content calculated over time t at Cartesian coordinates x, y and z (m). In this study, rainfall R ($m^3\ hr^{-1}$) is the source of water, and evaporation E ($m^3\ hr^{-1}$) and leachate L ($m^3\ hr^{-1}$) are the processes leading to water losses. Spatial gradients in pressure head h (m) drive flow, whereas the hydraulic conductivity K (m hr^{-1}), which is a function of h, controls its rate.

Two pore models were used to represent the hydraulic behavior of woodchips. The single pore model (SPM) describes the water retention ($\theta(h)$) and conductivity ($K(h)$) functions of a permeable media with a unimodal pore size distribution (Mualem, 1976; van Genuchten, 1980), whereas the dual pore model (DPM) considers two overlapping pore networks that are represented as the linear addition

of two weighted SPM-type water retentions (Durner, 1994). Functions describing changes in θ and K with *h* for the SPM are from van Genuchten (1980), and Mualem (1976), respectively

$$\theta(h) = \theta_r + \frac{\theta_s - \theta_r}{[1 + (\alpha h)^n]^m} \tag{3}$$

$$K(h) = K_s S_e^l \left[1 - (1 - S_e^{1/m})^m\right]^2 \tag{4}$$

where θ_r is the residual volumetric water content ($m^3\ m^{-3}$) after all flow ceases, θ_s is the saturated volumetric water content ($m^3\ m^{-3}$), α, n and m are fitting parameters related to the arrangement of the pore network ($\alpha > 0; n > 1; m = 1 - \frac{1}{n}$), K_s (m hr^{-1}) is the saturated hydraulic conductivity, S_e is the effective volumetric water content ($S_e = \frac{\theta(h) - \theta_r}{\theta_s - \theta_r}$; -) and l represents the tortuosity (-), which was fixed at 0.5.

The DPM pore model is parameterized similarly to the SPM, but includes another parameter w, a weighting factor that controls the partitioning of water between the dual pore subsystems (Durner, 1994).

$$\theta(h) = \theta_r + \frac{\theta_s - \theta_r}{\sum_{i=1}^{2} w_i [1 + (\alpha_i h)^{n_i}]^{m_i}} \tag{5}$$

$$K(h) = K_s \frac{\left(\sum_{i=1}^{2} w_i S_{ei}\right)^l \left[\sum_{i=1}^{2} w_i \alpha_i \left\{1 - (1 - S_{ei}^{1/m_i})^{m_i}\right\}\right]^2}{\left(\sum_{i=1}^{2} w_i \alpha_i\right)^2} \tag{6}$$

Each pore subsystem has its own values of α, n, m and w ($w_2 = 1 - w_1$) values, where the subscripts 1 and 2 denote properties for the pore subsystems assumed to be *between* and *within* the woodchip particles, respectively.

2.4 Materials & Methods

2.4.1 Field Experiment

A field experiment was conducted at the Burlington County Resource Recovery Complex (BCRRC) in Mansfield, New Jersey from May 25, 2012 to November 18, 2012. Data collected during this period is referred to as the Run 3 experiment in the related study by Kannepalli (2014).

Three woodchip piles were set up on 7.3 m diameter concrete pads. The high point of each pad was at the center and from there was graded 1° towards a 0.6 m wide swale encircling the perimeter. Each swale drained leachate into two 7.6 cm poly vinyl floor drains that transported it to a collection bucket located in a nearby shed (Fig. 2.1A). Leachate volumes were measured separately for each pile via 1-L tipping buckets and were recorded in 10-minute intervals to a CR1000 data logger (Campbell Scientific, Inc., Logan, UT, USA).

The woodchips used to construct each pile were processed onsite at BCRRC from trees, branches, brush, and twigs sourced primarily in state. To setup each pile, three loader buckets filled with specific mixtures of woodchips were placed in a truck, which was weighed using an onsite truck scale to estimate the mass of the piles. The woodchip piles are identified as L1, R2 and F2 (Fig. 2.1B), where the letters indicate their position relative to viewing them from the shed housing the leachate collection system (Left, Right and Far, respectively), and the numbers indicate whether the woodchips were ground once (1) or twice (2).

Representative samples from each pile were collected according to the Test Methods for the Examination of Composting and Compost (US Composting Council, 2010) and are described in further detail in Kannepalli (2014). The particle size distribution for each of the three piles was determined in triplicate by mechanically sieving 2 L samples of woodchips (ASABE, 2006) through a set of 10 US

Standard sieves with openings (mm) of 25.40, 19.05, 9.53, 5.66, 2.83, 1.41, 0.59, 0.30, 0.15, and 0.06. The mass percent of woodchips $F(d)$ retained on each sieve was fitted to a sigmoidal function (Haverkamp and Parlange, 1994)

$$F(d) = \frac{1}{\left[1 + (\frac{I_d}{d})^{k_d}\right]^{(1-\frac{1}{k_d})}} \tag{7}$$

where d (µm) is the particle diameter, and I_d and k_d are fitting parameters. The median particle diameter (d_{50}; µm) was calculated from Eq. 7 by solving for d when $F(d) = 0.5$. The geometric mean diameter (d_g; µm) was calculated as

$$d_g = \prod_{i=0}^{11} d_{gi}^{fi} \tag{8}$$

where d_{gi} is the geometric mean (µm) between the ith and $(i+1)^{th}$ sieve openings and f_i is the mass fraction that is retained on the ith sieve. The lower (i=0) and upper bound ($(i+1)^{th}$=11) to calculate d_{gi} for the smallest and largest sieve diameters were assumed to be 0.001 mm and 50.8 mm, respectively.

The dry bulk density (ρ_d; Mg m^{-3}) was determined in the laboratory for the once and twice ground woodchip mixtures by dropping a calibrated container with one kilogram of loosely packed air-dried material 15 times from a height of 15 cm onto a rubber mat (ASAE, 1998). The average depth of the settled material after the last drop was used to estimate the sample's volume. On the same day the piles were assembled, the initial volumetric moisture content θ_{init} (m^3 m^{-3}) of the woodchips in each pile was determined by weighing the samples before and after they were dried in an oven at 105° C for 24 hours and then using ρ_d and the density of water to convert the mass of water lost into a volume (ASAE, 1998).

Rotating laser surveying equipment (CST/berger Lasermark Wizard LM 30 series, Watseka, IL, USA) was used to establish a reference level above each pile. The distance between the surface of the pile and the reference level was used to determine the height of the pile at 49 points corresponding to the intersection points of a 6 x 6 grid covering an area of 7.2 x 7.2 m^2. The height (m) of each of the 36 square cells (1.2 x 1.2 m^2) in the grid was approximated as the average measured height of its four corners. The volume of woodchips (m^3) occupying each cell was estimated by multiplying its average height by its area. The volume of each pile (m^3) was taken as the sum of the estimated woodchip volumes occupying the 36 rectangular cells within the surveyed area.

2.4.2 Model Setup

Statistical differences between the hourly leachate measurements from the experimental piles were tested at the 95% confidence level with a two-sample non-parametric Kolmogorov-Smirnov (KS) test, which computes the maximum vertical distance, D between the empirical cumulative distributions of two samples to discern differences (Arnold and Emerson, 2011).

For the rest of the statistical analyses in this study, leachate measurements were compiled into 6-hour records due to a latency noticed between the response of the leachate collection system and the onset of precipitation. This was deemed a sufficient amount of time for leachate to travel through the collection system and to be measured by the tipping bucket while still preserving key temporal features in the data set. Also in terms of model optimization and performance evaluation, it was considered more practical to be able to accurately predict total leachate over the course of a storm, rather than predict it for a given hour within a storm. Leachate measurements from the L1 and R2 piles were used as training datasets for optimizing the SPM and DPM models, while measurements taken from the F2 pile were used as a validation set.

Three-dimensional model domains representing the L1, R2 and F2 piles were created in the HYDRUS 3D-General graphical user interface (HYDRUS 2D/3D, PC-Progress, Prague, CZ). Each domain was composed of two geo-objects: (1) the pile was defined by using the x, y and z coordinates corresponding to the average height estimates acquired from laser measurements to create a surface of stitched together quadrangles; and (2) the swale encircling the pile was defined as an annulus with a uniform depth of 3.5 cm (Fig. 2.1C). The swale was included in HYDRUS simulations as part of the capture area influencing leachate measurements and it was given fixed water retention properties for Portland cement (Table 2.1) and consistent with an SPM-type water retention (Savage and Janssen, 1997; Leech *et al.,* 2006; Leech *et al.,* 2008).

The base of the stockpile was set as a no flux boundary condition (BC) and graded according to the construction plans. A seepage face BC was assigned at the bottom and outer edge of the swale, which was designed to release outflow (*i.e.,* leachate) only when the one-element layer became saturated ($h \geq 0$). The hourly flux of leachate across the seepage face was summed every 6-hours for evaluating model performances.

A time-variable atmospheric BC was applied to the topmost surfaces and it was assigned hourly precipitation values according to the hourly measurements acquired from the Mansfield, New Jersey weather station, which is part of a state-operated climate network and is located onsite at BCRRC. Precipitation was also measured next to the concrete pad (Fig. 2.1) with a 20.3 cm siphoning tipping bucket rain gauge (Intermountain Environmental, Inc., Logan); this was used to verify that the local precipitation record was similar to that measured by the Mansfield station.

Meteorological conditions acquired from the Mansfield station were used to estimate the hourly potential evaporation rate assuming well-watered conditions following the FAO-56 Penman Monteith method (Liukko and Elowsson, 1997; Allen *et al.,* 1998). Since woodchip stockpiles could not sustain the

potential evaporation rate because they were not constantly saturated, the actual hourly evaporation rate was computed by multiplying the potential evaporation rate by a dimensionless coefficient to more realistically reflect evaporation from a surface with less than 10% albedo and limited moisture conditions (Allen *et al.,* 2005). Additionally, the evaporation rate was increased by 10% to account for enhanced biological heat production occurring near the center of the piles that was expected to increase the flux of energy towards their cooler evaporative surfaces, ultimately enhancing the evaporation rate (Bendz and Bengtsson, 1995).

2.4.3 Model Optimization

The SPM and DPM were optimized using Bayesian inference, which works by treating unknown model parameters as random variables x that are each assigned a predefined prior probability distribution $p(x)$. The $p(x)$ represents what is known about a particular random variable x before new data Y, which is somehow conditionally dependent on x, is observed. The new observations of Y can then be used to update $p(x)$, in order to obtain a posterior probability distribution $p(x|Y)$.

In the Bayesian formalism, the $p(x|Y)$ is obtained by evaluating a likelihood function $L(Y|x)$, which quantifies the model's ability to explain the observations of Y provided a value for x.

$$p(x|Y) \propto p(x)L(Y|x) \tag{9}$$

Posterior distributions $p(x|Y)$ are inferred by generating and evaluating thousands of combinations of x values using Eq. 9 (Gelman *et al.,* 2015). The number of model parameters subjected to inference was reduced to only those that were considered estimable based on their influence on simulating leachate generation $\hat{Y}$ (m^3 per 6 hours).

The parameter ranking algorithm coded in MatLab® (MathWorks, Natick, MA, USA) by Yao *et al.* (2003) was used to quantify parameter estimability. First, sensitivity coefficients $I_{t,k}$ were calculated for

the kth hydraulic parameter p at each time step t. The $I_{t,k}$ represents the partial differential of the change in $\hat{Y}$ with respect to changes in p_k when the rest of the model parameters are kept constant. It can be approximated using a centered finite difference approach (Yao *et al.,* 2003)

$$I_{t,k} = \frac{\partial \hat{Y}}{\partial p_k} \approx \frac{\hat{Y}^+ - \hat{Y}^-}{2\Delta p_k} \tag{10}$$

where $\hat{Y}^+$and $\hat{Y}^-$ are the simulated leachate volumes at t when p_k is increased and decreased by 5%, respectively. The 2Δ in the denominator reflects an overall 10% change and is therefore equal to 0.1. To make relative comparisons between parameters, $I_{t,k}$ was normalized by p_k and the mean simulated leachate volume $\bar{Y}$ when p_k is not increased/decreased (Hamby, 1994).

$$I_{t,k\ norm} = \frac{p_k}{\bar{Y}} I_{t,k} \tag{11}$$

A normalized sensitivity coefficient $I_{t,k\ norm}$ was computed for all hydraulic flow parameters included in the analysis and a sensitivity matrix Z with $t\ x\ k$ dimensions was constructed (in our case t=631 and k=4 (SPM) or k=7 (DPM)).

$$Z = \begin{bmatrix} I_{1,1\ norm} & I_{1,2\ norm} & \cdots & I_{1,k\ norm} \\ I_{2,1\ norm} & I_{2,2\ norm} & \cdots & I_{2,k\ norm} \\ \cdots & \cdots & \cdots & \cdots \\ I_{t,1\ norm} & I_{t,2\ norm} & \cdots & I_{t,k\ norm} \end{bmatrix} \tag{12}$$

The orthogonalization method (Yao *et al.,* 2003) was used to rank the k parameter constituents of Z. Residual water content (θ_r) for woodchips was assumed to be 0 cm^3cm^{-3} (Eq. 3-6), thus this parameter was left out of estimability analyses and fixed for optimization. This decision is corroborated by Ngo *et al.* (2013) who showed θ_r was consistently ranked the least estimable SPM parameter, regardless of the response variable used to evaluate its estimability. The tortuosity parameter l (Eq. 4, 6) was also left out of the analysis and fixed at 0.5 as it was in Subroy *et al.* (2014) and other hydraulic property optimizations for solid wastes (Scicchitano 2010; Han *et al.*, 2011).

The flow parameters of the SPM (k=4) and DPM (k=7) models were ranked six separate times using different combinations of parameter values presented in Subroy *et al.* (2014). The average parameter rankings for the SPM and DPM were then used to determine which parameters should be inferred or fixed at a previously measured value. The values of these fixed parameters were determined by running the HYDRUS 3D woodchip pile models with the optimized parameter sets from 1D MSO experiments (Subroy *et al.*, 2014) and selecting the set that best matched the leachate data from the three experimental piles.

A MatLab® coded version of the DiffeRential Evolution Adaptive Metropolis ($DREAM_{ZS}$) Bayesian MCMC algorithm (Vrugt, 2016) was used to optimize the estimable subsets of SPM and DPM flow parameters using measurements from stockpiles L1 and R2. Each parameter subjected to inference was assigned an informative prior distribution (Table 2.1) that was approximately based on the posterior distributions from 1D MSO experiments (Subroy *et al.,* 2014). Parameters were conditioned using a normal likelihood function with 6-hour measurements of leachate that were assumed to have homoscedastic measurement error. The MCMC sampler was programmed to run three Markov chains in parallel across the local distributed computing network for a total of 15,000 chain generations, resulting in a total of 45,000 MCMC samples.

The last 1,500 samples from each chain were accepted as part of the posterior distribution, but only if the potential scale reduction factor $\widehat{R}$ calculated for the three chains was less than 1.2 (Gelman and Rubin, 1992). Otherwise, $DREAM_{ZS}$ was run another 1,000 chain generations until that condition was met.

2.4.4 Posterior Analysis

For the SPM and DPM models, differences between the inferred hydraulic parameters for the once (L1) and twice (R2) ground woodchip mixtures were compared by subtracting the posterior

samples of each hydraulic parameter from one another. The resulting distribution of posterior parameter contrasts were summarized by their interquartile range (IQR): a continuous range of values between the 25th and 75th percentiles. If zero is contained in an IQR, then that parameter's posterior distributions were sufficiently overlapping that they were deemed statistically similar to one another. If zero was not contained in the IQR, then the posterior distributions were disjoint enough that they were considered statistically different.

Additional sets of SPM and DPM hydraulic parameters were created by combining the posterior samples for the L1 and R2 woodchip mixtures. These new sets were formulated as multivariate Gaussian distributions parameterized by a vector of the mean parameter values (SPM: 3; DPM: 4) and a symmetrical covariance matrix (SPM: 3x3; DPM: 4x4). The main advantage of using a multivariate Gaussian distribution is to account for possible correlations between the water retention parameters (Scharnagl *et al.,* 2011).

2.4.5 Model Performance and Validation

The performance of the optimized SPM and DPM hydraulic parameter sets for the L1 and R2 woodchip piles were evaluated by randomly sampling 100 parameter combinations from the posterior distributions inferred by DREAM$_{ZS}$ and running them forward in HYDRUS 3D.

The performance of each forward simulation was evaluated with the Nash-Sutcliffe efficiency index (E_f) (Nash and Sutcliffe, 1970)

$$E_f = 1 - \frac{\sum_{t=1}^{N}(\widehat{Y}_t - Y_t)^2}{\sum(Y_t - \bar{\bar{Y}})^2} \tag{13}$$

where $\widehat{Y}_t$ and Y_t are the predicted and measured values of 6-hour leachate (L) at t, $\bar{\bar{Y}}$ is the average of the 6-hour leachate measurements and N is the total number of 6-hour measurements (N=631). The root mean square error ($RMSE$) was also computed for each forward HYDRUS 3D simulation.

$$RMSE = \sqrt{\frac{\sum_{t=1}^{N}(\hat{Y}_t - Y_t)^2}{N}} \quad (14)$$

The 6-hour intervals where no precipitation occurred and no leachate was generated were also included in the calculation of E_f and $RMSE$.

Leachate measurements from the F2 pile (not included in the optimization) were used to validate the optimized SPM and DPM parameters. A set of 100 randomly selected samples from the inferred posterior distributions for the R2 woodchips were used to simulate leachate from the F2 pile domain. The performance of each parameter combination was evaluated with E_f and $RMSE$. The combined multivariate parameter distributions were also validated based on their ability to simulate leachate generation in the HYDRUS 3D domain representing the F2 woodchip pile.

2.5 Results and Discussion

A summary of the physical characteristics of the experimental piles and the woodchip materials used to construct them are presented in Table 2.2. Given the asymmetrical cuboidal shape of the woodchip particles, the d_g and d_{50} values were taken as a representation of particle length rather than diameter because this dimension was more likely to prevent the particles from passing through the sieves. The size of the woodchips ground once (L1) were about double the size of the woodchips ground twice (R2 and F2). The finer R2 and F2 woodchip mixtures also had a more homogenized particle size distribution than the coarser L1 woodchip mixture (Table 2.2). Both the once and twice ground woodchips were relatively fine in texture compared to the range of about 1 to 8 mm in d_g values recorded by Subroy *et al.* (2014) and the range of d_{50} (~7-25 mm) recorded throughout the literature (Ima and Mann, 2007; Chun *et al.,* 2009; Christianson *et al.,* 2010; Ghane *et al.,* 2014; 2016).

Over the course of the experimental period the shape and volume of the woodchip piles noticeably changed as materials settled and degraded over time (Kannepalli, 2014). The woodchip

particle size distributions were also likely altered during this period (Ghane *et al.* 2014). Morphological changes of the piles and their particle size distributions over time were not considered in this study, but they could potentially influence the hydraulic behavior of the materials and leachate generation.

In total, there were 29 storm events that produced leachate in the experimental period (Fig. 2.2). The average amount of rainfall per event was 1.98 cm and the average hourly precipitation intensity was 0.25 cm hr^{-1}, with standard deviations of 1.51 cm and 0.41 cm hr^{-1}, respectively. The L1 woodchip pile leached more than the fine R2 and F2 piles, although according to the results of the Kolmogorov-Smirnov test there were no significant differences ($p < 0.05$) between the three leachate datasets (D values computed for the L1-R2, L1-F2 and R2-F2 comparisons were 0.053, 0.043 and 0.064, respectively).

There were two storm events (June 22-23 and July 15, 2016) that produced substantial leachate volumes from the R2 and F2 piles, but none from the L1 pile. Likewise, two different storm events on July 27-28 and August 10, 2016 produced substantial leachate in the L1 and R2 piles, but none was recorded for the F2 pile (Figure 2.2). Since there were no attributable sources for these lacks of response, the leachate data was taken as is for the optimization (L1 woodchips).

2.5.1 Parameter Estimability

Estimability analysis was used to determine which parameters should be subjected to inference and which could be fixed. The parameter rankings were not always consistent (Table 2.3), likely because Eq. 10 employs a local linear difference method to approximate the nonlinear $\frac{\partial \hat{Y}}{\partial p_k}$ relationship. The complexity of estimating $\frac{\partial \hat{Y}}{\partial p_k}$ was likely exacerbated by mutual dependencies between some of the SPM and DPM water retention parameters (Hopmans and Simunek, 1999; Larsbo and Jarvis, 2006), as well as by the difficulty of estimating water retention parameters based on outflow data alone (Vrugt *et al.,*

2001; Ngo *et al.,* 2013). Thus, multiple different sets of parameters needed to be evaluated to ensure that the rankings were actually reflective of parameter influence and not just a result of poor initial parameter guesses (McLean and McAuley, 2012).

The parameters θ_s and n were consistently ranked the most estimable for the SPM, while α and K_s were ranked less estimable (Table 2.3). Since in this study θ_r was given a value of 0, θ_s represents the total porosity and defines the overall capacity of the woodchips to retain stormwater. The exponent n defines the steepness of the water retention and hydraulic conductivity relationships, thus manipulating n changes the range of h where flow is substantial enough to generate leachate.

The ranked estimability results for the DPM were not as conclusive as for the SPM (Table 2.3). On average, θ_s and n_1 were ranked the most estimable hydraulic parameters followed by the partitioning parameter w_2. The magnitude of w_2 reflects how much influence the porosity subsystems with wider (α_1/n_1) and narrower (α_2/n_2) diameters have on the water retention/conductivity relationships. Since the wider diameter pores have greater conductivity they will have a greater influence over rapid leachate generation during wetting events. In contrast, the narrower pores have greater retentive ability and will transmit water slower.

The results of the estimability analysis combined with the mathematical underpinning of how each parameter influences the water retention relationship aided the decision to infer θ_s, n and α for the SPM and θ_s, n_1, α_1 and w_2 for the DPM. Fixing α_2 and n_2 at previously measured values (Subroy *et al.*, 2014) while inferring w_2 left it to the optimization algorithm DREAM$_{ZS}$ to identify whether the presence of a second pore subsystem was detectable using leachate generation data as evidence in the Bayesian inference.

2.5.2 Parameter Inference

The inferred posterior distributions for each hydraulic pore model (SPM/DPM) and each woodchip mixture (once ground L1/twice ground R2) are presented in Table 2.4, along with their *maximum a posteriori* (MAP) estimates, which are the set of parameters that maximized Eq. 9. Except for the R2 DPM optimization that required 21,000 MCMC samples to achieve convergence, the rest of the models required 15,000.

Ideally the MCMC sampler would have been allotted many more chain generations to yield more robust posterior parameter estimates; however, due to the complexity of simulating unsaturated flow in three-dimensions, each model simulation took up to ~20 minutes. This prompted the decision to bound the proposal space and use informative prior distributions (Table 2.1) so that only the most viable regions of the posterior parameter spaces were explored (Scharnagl *et al.,* 2011). Still the MCMC acceptance rates were low (about 10%), which consequently resulted in sparse posterior distributions, albeit "stably" converged based on the diagnostic $\widehat{R} < 1.2$.

The posterior distributions of the inferred hydraulic parameters for the L1 and R2 piles (Table 2.4) were subtracted from one another to examine for differences between the once and twice ground woodchip mixtures (Fig. 2.3). If the IQR of a particular parameter contrast contained 0, the two posteriors were considered statistically similar to one another. The only contrast that yielded a statistical difference was θ_s for the SPM as the finer woodchips in the R2 pile had greater inferred porosity than the coarser woodchips in the L1 pile (Table 2.4). For the DPM, however, the posterior distributions for the once (L1) and twice (R2) ground woodchips were similar enough that they reasonably could be combined, effectively doubling the posterior sample size of each parameter (Fig. 2.4).

Quantifying w_2 provided insight on whether the increased complexity of the DPM is justified (w_2 is sufficiently greater than 0) or if the assumptions of an SPM-type water retention are admissible for simulating leachate generation (w_2 is near 0). The MAP estimates of w_2 were 0.04 and 0.1 for the L1 and R2 woodchip mixtures, respectively (Table 2.4). At the same time, approximately 27% of the combined posterior density for w_2 was less than 0.02 (Fig. 2.4). The variances of posterior distributions for w_2 were substantially higher than for any of the other inferred parameter distributions (Table 2.4). This issue is a result of different parameter combinations leading to statistically similar model likelihood, in turn making it difficult to identify which parameter combinations are describing the most 'true' representation of the water retention behavior (Hopmans and Simunek, 1999).

The correlation (cor) and covariance (cov) of the combined posterior distributions (L1+R2) for the DPM water retention parameters is visible in Figure 2.4. Most strikingly there is a dependency between α_1-n_1, θ_s-α_1, n_1-w_2 and α_1-w_2; while θ_s-w_2 and θ_s-n_1 are less dependent. The cor/cov structure of the combined posterior distributions (L1+R2) for the SPM (data not shown) are θ_s-n (cor: 0.11/ cov: 5.8E-5), α-n (cor: 0.15/ cov: 3.6E-5) and α-θ_s (cor: 0.35/ cov: 5.7E-4). This evidence of an apparent correlation structure supports using a multivariate Gaussian distribution to summarize the combined posterior probability distributions (L1+R2) for the SPM and DPM parameters (Scharnagl *et al.,* 2011).

2.5.3 Model Performance

The 95% confidence intervals (*i.e.,* the range between the 2.5 and 97.5 percentiles) for the predicted cumulative volumes of leachate by the SPM and DPM are strikingly similar (Fig. 2.5). In fact, the SPM has a tighter band of confidence than the DPM, which is a direct result of the SPM's posterior parameter estimates having less uncertainty than the DPMs (Table 2.4).

The goodness-of-fit statistics in Table 2.5 were calculated after simulating 100 randomly drawn parameter combinations in HYDRUS 3D from the univariate (Table 2.4) and combined (L1+R2)

multivariate posterior distributions. The metric E_f ranges from -1 to 1 where more positive values reflect unbiased model predictions, negative values indicate biased predictions and a value of 0 indicates the model is as good a predictor as $\bar{Y}$ (Nash and Sutcliffe, 1970).

Overall the optimized parameter distributions for both the SPM and DPM were more than satisfactorily able to predict leachate generation from the L1, R2 and F2 piles (Table 2.5; Fig. 2.6). This is especially true after removing the two leachate anomalies measured in the L1 and F2 piles (see Section 2.5). Using the R2 parameter sets to predict leachate generation from the F2 pile showed that the optimized parameters can be extrapolated for use in similar woodchip piles.

Examining the residuals between the measured and simulated leachate for the F2 pile show that the SPM under-predicted leachate by about 25% and the DPM by about 23% (Fig. 2.6). For the L1 and R2 piles, these values for the SPM/DPM were 27%/26% and 14%/13%, respectively (data not shown).

Leachate predicted with SPM and DPM from the L1 and R2 piles during different 6-hour storm intensities was evaluated by classifying storms into small ($0 < P \leq 0.25$ cm), medium ($0.25 < P \leq 1$ cm) and large events ($P > 1$ cm). Generally, the variance of the residuals increased as storm intensity increased (Fig. 2.7). For small and medium events, the model residuals are Gaussian-distributed and centered about 0. For large storm events, the residuals are negatively biased and there is much more uncertainty; however, it is difficult to determine whether the bias is real or if measurement errors increased when rainfall intensified due to unintended collection of surface runoff from other parts of the concrete pad.

Randomly sampling from the combined multivariate distributions did not necessarily improve the goodness-of-fit (Table 2.5); however, using the multivariate distribution decreased the number of DPM parameter combinations that caused HYDRUS to crash from numerical instabilities. About 23% of the randomly selected parameter combinations from the univariate DPM posterior distributions caused

HYDRUS to crash, in comparison to the 5% when the multivariate DPM posterior distribution was sampled from. The SPM did not have the same issue with HYDRUS crashing mid-simulation from faulty parameter combinations.

2.5.4 Future Improvements

A better understanding of the internal flow dynamics is important for minimizing environmental risks associated with the open storage of woodchips, as well as maintaining the quality of the stockpiled materials (Afzal *et al.,* 2009; Lenz *et al.,* 2015; Lin and Pan, 2015; Hofmann *et al.,* 2017). Time series measurements of water content obtained with a reflectometer (Amato *et al.,* 2019; Kannepalli, 2014) should be incorporated to analyze flow patterns within woodchip piles and investigate the model's ability to simulate them. This is particularly important because the woodchips were assumed to be homogenously distributed throughout the pile and the flow through them was considered isotropic. However, it is likely the natural stratification of particle sizes in sloped pile systems would cause anisotropic flow behavior, which affects leachate generation (Molson *et al.,* 2005; Fala *et al.,* 2005; Namaghi *et al.,* 2015). Furthermore, using spatially distributed measurements of water content within the woodchip piles as supplementary model evidence (Eq. 9) will likely improve the identifiability of the hydraulic parameters and ultimately the physical accuracy of the flow model.

Future emphasis should also be placed on understanding how hydraulic properties of woodchips change with time as the piles become more degraded, more compacted and woodchip particle sizes decrease. As a result of degradation processes, older woodchips have been shown to have less intrinsic permeability and also a greater ability to retain moisture than fresh woodchips (Ghane *et al.,* 2014; 2016).

2.6 Conclusions

Simulating transient flow through woodchip piles to optimize the SPM and DPM models in HYDRUS 3D was CPU-intensive. Reducing the number of parameters subjected to inference and using informative prior distributions helped speed up convergence, although it influenced the acceptance criteria of the MCMC sampler. Still the optimized SPM and DPM hydraulic parameter sets were more than adequately able to simulate 6-hour leachate generation from piles of once and twice ground woodchip mixtures. There were no significant differences found between the measured leachate datasets for the experimental piles; the optimized SPM and DPM hydraulic parameter sets for the fine and coarse woodchip mixtures were also statistically similar. Overall the SPM had similar predictive capability to the DPM, but it did not have issues with numerical instability that caused the simulations to crash. Thus for future simulations it is recommended to use the SPM. The optimized hydraulic parameters for woodchips provided in this study could be used to assess how different geometric pile configurations and management strategies impact the quantity and quality of leachate generation.

2.7 References

Amato, M. T., Subroy, V., Giménez, D., Strom, P. F., Krogmann, U., 2019. Dielectric permittivity-water content relationships in woodchips: Particle size and temperature effects. *J. Hydrol. 572*, 251-260.

Afzal, M.T., Bedane, A.H., Sokhansanj, S., Mahmood, W., 2009. Storage of comminuted and uncomminuted forest biomass and its effect on fuel quality. *BioResour. 5*(1), 55-69.

Allen, R. G., Pereira, L. S., Raes, D., Smith, M., 1998. Crop evapotranspiration: Guidelines for computing crop water requirements. FAO Drainage and Irrigation Paper 56, Food and Agriculture Organization, Rome.

Allen, R. G., Pruitt, W. O., Raes, D., Smith, M., Pereira, L. S., 2005. Estimating evaporation from bare soil and the crop coefficient for the initial period using common soils information. *J. Irrig. Drain. Eng.* 131(1), 14-23.

Arnold, T. B., Emerson, J. W., 2011. Nonparametric goodness-of-fit tests for discrete null distributions. *R J.* 3, 34–39.

ASABE, 2006. Method of determining and expressing particle size of chopped forage materials by screening. American Society of Agricultural and Biological Engineers, St. Joseph, MI, USA. pp. 619-621.

ASAE, 1998. Cubes, pellets and crumbles- Definitions and methods for determining density, durability and moisture content. American Society of Agricultural Engineers, St. Joseph, MI, USA. pp. 525-527.

Bedane, A. H., Afzal, M. T., Sokhansanj, S., 2011. Simulation of temperature and moisture changes during storage of woody biomass owing to weather variability. *Biomas Bioenergy. 35*(7), 3147-3151.

Bendz, D., Bengtsson, L., 1996. Evaporation from an active, uncovered landfill. *J. Hydrol. 182*(1-4), 143-155.

Christianson, L., Castelló, A., Christianson, R., Helmers, M., Bhandari, A., 2010. Technical Note: Hydraulic Property Determination of Denitrifying Bioreactor Fill Media. *App. Eng. Agr.*, 26(5), 849-854.

Chun, J., Cooke, R., Eheart, J., Kang, M., 2009. Estimation of flow and transport parameters for woodchip-based bioreactors: I. laboratory-scale bioreactor. *Biosyst. Eng.* 104(3), 384-395.

Duncan, O. J., Tollner, E. W., Ssegane, H., 2013. An instantaneous unit hydrograph for estimating runoff from windrow composting pads. *App. Eng. Agr., 29*(2), 209-223.

Durner, W., 1994. Hydraulic conductivity estimation for soils with heterogeneous pore structure. *Water Resour. Res.* 30(2), 211-223.

Fala, O., Molson, J., Aubertin, M., Bussière, B., 2005. Numerical modelling of flow and capillary barrier effects in unsaturated waste rock piles. *Mine Water Environ.* 24(4), 172-185.

Falk, R.H., McKeever, D.B., 2004. Recovering wood for reuse and recycling: a United States perspective, in: European COST E31 Conference-Management of Recovered Wood: Recycling, Bioenergy and Other Options. University Studio Press, Thessaloniki, Greece, pp. 29–40.

Ferrero, F., Lohrer, C., Schmidt, B. M., Noll, M., Malow, M., 2009. A mathematical model to predict the heating-up of large-scale wood piles. *J. Loss Prevent. Proc.* 22(4), 439-448.

Gelman, A., Rubin, D.B., 1992. Inference from iterative simulation using multiple sequences. *Stat. Sci. 7*(4), 457-472.

Gelman, A., Carlin, J.B., Stern, H.S., Dunson, D.B., Vehtari, A., Rubin, D.B., 2015. *Bayesian data analysis*, CRC Press, Florida, 3rd ed.

Gerke, H. H., Genuchten, M. Th., 1993. A dual-porosity model for simulating the preferential movement of water and solutes in structured porous media. *Water Resour. Res. 29*(2), 305-319.

Ghane, E., Fausey, N. R., Brown, L. C. 2014. Non-Darcy flow of water through woodchip media. *J. Hydrol. 519*, 3400-3409.

Ghane, E., Feyereisen, G. W., Rosen, C. J., 2016. Non-linear hydraulic properties of woodchips necessary to design denitrification beds. *J. Hydrol. 542*, 463-473.

Hamby, D. M., 1994. A review of techniques for parameter sensitivity analysis of environmental models. *Environ. Monit. Assess.* 32(2): 135-154.

Han, B., Scicchitano, V., Imhoff, P. T., 2011. Measuring fluid flow properties of waste and assessing alternative conceptual models of pore structure. *Waste Manage.* 31(3), 445-456.

Haverkamp, R., Parlange, J., 1986. Predicting the water-retention curve from particle-size distribution. *Soil Sci. 142*(6), 325-339.

Hedmark, A., Scholz, M., 2008. Review of environmental effects and treatment of runoff from storage and handling of wood. *Bioresour. Technol.* 99(14), 5997-6009

Hofmann, N., Mendel, T., Schulmeyer, F., Kuptz, D., Borchert, H., Hartmann, H., 2017. Drying effects and dry matter losses during seasonal storage of spruce wood chips under practical conditions. *Biomass Bioenergy*. 111, 196-205.

Hopmans, J.W., Šimůnek., J., 1999. Review of inverse estimation of soil hydraulic properties. pp. 643–659. In van Genuchten *et al.* (ed.) *Characterization and measurement of the hydraulic properties of unsaturated porous media*. Proc. Int. Workshop., Riverside, CA. 22–24 Oct. 1997. U.S. Salinity Lab., Riverside, CA

Ima, C.S., Mann, D.D., 2007. Physical properties of woodchip: compost mixtures used as biofilter media. Agricultural Engineering International: the CIGR Journal, IX. Manuscript BC 07 005

Jaynes, D. B., Moorman, T. B., Parkin, T. B., Kaspar, T. C., 2016. Simulating Woodchip Bioreactor Performance Using a Dual-Porosity Model. Journal of Environment Quality, 45(3), 830

Kalaba, L., Wilson, B. G., Haralampides, K., 2007. A stormwater runoff model for open windrow composting sites. *Compost Sci. Util.* 15(3), 142-150.

Kannepalli, S., Strom, P.F., Krogmann, U., Subroy, V., Giménez, D., Miskewitz, R., 2016. Characterization of wood mulch and leachate/runoff from three wood recycling facilities. *J. Environ. Manage*. 182, 421-428.

Kannepalli, S., 2014. *Environmental issues in organics recycling: Reed bed biosolids reuse and leachate from wood mulch stockpiles*. (*Doctoral Dissertation*) Rutgers, The State University of New Jersey, New Brunswick, New Jersey

Khire, M. V., Mukherjee, M., 2007. Leachate injection using vertical wells in bioreactor landfills. *Waste Manage.* 27(9), 1233-1247.

King, M., Macdonald, G., Hutchinson, M., Seekings, B., 2014. A comparison of the quantity and quality of leachate generated by five compost feedstocks exposed to simulated rainfall. *J. Solid Waste Technol. Manage. 40*(1), 57-69.

Laloy, E., Weynants, M., Bielders, C., Vanclooster, M., Javaux, M., 2010. How efficient are one-dimensional models to reproduce the hydrodynamic behavior of structured soils subjected to multi-step outflow experiments? *J. Hydrol*. 393(1-2), 37-52.

Larsbo, M., Jarvis, N., 2006. Information content of measurements from tracer microlysimeter experiments designed for parameter identification in dual-permeability models. *J. Hydrol.325*(1-4), 273-287.

Leech, C., Lockington, D., Hooten, D., 2006. Estimation of water retention curve from mercury intrusion porosimetry and van Genuchten model. *ACI Struct. J. 103*(2).

Leech, C., Lockington, D., Hooten, D., Galloway, G., Cowin, G., Dux, P., 2008. Validation of Mualem's conductivity model and prediction of saturated permeability from sorptivity. *ACI Mater. J. 105*(1).

Lenz, H., Idler, C., Hartung, E., Pecenka, R., 2015. Open-air storage of fine and coarse wood chips of poplar from short rotation coppice in covered piles. *Biomass Bioener*gy. 83, 269-277.

Li, X., Koseki, H., Momota, M., 2006. Evaluation of danger from fermentation-induced spontaneous ignition of wood chips. *J. Hazard. Mater. 135*(1-3), 15-20.

Lin, Y., Pan, F., 2015. Monitoring Woody Biomass Chips Quality Change during Field Storage in Michigan. *For. Prod. J. 65*(7-8), 327-336.

Liukko, K., Elowsson, T., 1997. Potential and measured evaporation in saw timber piles of *pinus sylvestris*. *Scand. J. Forest Res.* 12(1), 57-64.

Mclean, K. A., Mcauley, K. B., 2011. Mathematical modelling of chemical processes-obtaining the best model predictions and parameter estimates using identifiability and estimability procedures. *Can. J. Chem. Eng.* 90(2), 351-366.

Molson, J., Fala, O., Aubertin, M., Bussière, B., 2005. Numerical simulations of pyrite oxidation and acid mine drainage in unsaturated waste rock piles. *J. Contam. Hydrol.* 78(4), 343-371.

Mualem, Y., 1976. A new model for predicting the hydraulic conductivity of unsaturated porous media. *Water Resour. Res.* 12(3), 513-522.

Nash, J., Sutcliffe, J., 1970. River flow forecasting through conceptual models part I — A discussion of principles. *J. Hydrol.* 10(3), 282-290.

Namaghi, H. H., Li, S., Jiang, L., 2015. Numerical simulation of water flow in a large waste rock pile, Haizhou coal mine, China. *Model. Earth Syst. Environ*. 1(1-2).

Ngo, V. V., Gerke, H. H., & Badorreck, A., 2014. Estimability analysis for optimization of hysteretic soil hydraulic parameters using data of a field irrigation experiment. *Transport Porous Med.* 103(3), 535-562.

Ngo, V. V., Latifi, M. A., & Simonnot, M., 2013. Estimability analysis and optimisation of soil hydraulic parameters from field lysimeter data. *Transport Porous Med.* 98(2), 485-504.

Safari, E., Ghazizade, M. J., Abdoli, M. A., 2012. A performance-based method for calculating the design thickness of compacted clay liners exposed to high strength leachate under simulated landfill conditions. *Waste Manage. Res.* 30(9), 898-907.

Savage, B. M., Janssen, D. J., 1997. Soil physics principles validated for use in predicting unsaturated moisture movement in portland cement concrete. *ACI Mater. J. 94*(1).

Scicchitano, V., 2010. Estimating hydraulic properties of landfill waste using multistep drainage experiments. M.S. Thesis. University of Delaware, Newark, DE, USA.

Scharnagl, B., Vrugt, J. A., Vereecken, H., & Herbst, M., 2011. Inverse modelling of in situ soil water dynamics: investigating the effect of different prior distributions of the soil hydraulic parameters. *Hydrol. Earth Syst. Sci.* 15(10), 3043-3059.

Seng, B., Kaneko, H., Hirayama, K., Katayama-Hirayama, K., 2012. Development of water movement model as a module of moisture content simulation in static pile composting. *Environ. Technol.* 33(15), 1685-1694.

Šimůnek, J., van Genuchten, M.Th., Sejna, M., 2012. The HYDRUS software package for Simulating the two- and three-dimensional movement of water, heat, and multiple solutes in variably-saturated porous media. Technical Manual, Version 2.0, PC Progress, Prague, Czech Republic

Solid Waste Association of North America, 2002. Successful approaches to recycling urban wood waste. Madison, WI: U.S. Department of Agriculture, Forest Service, Forest Products Laboratory. Gen. Tech. Rep. FPL-GTR-133. pp. 20.

Subroy, V., Giménez, D., Qin, M., Krogmann, U., Strom, P. F., Miskewitz, R. J. (2014). Hydraulic properties of coarsely and finely ground woodchips. *J. Hydrol. 517*, 201-212.

Svensson, H., Marques, M., Kaczala, F., Hogland, W., 2013. Leaching patterns from wood of different tree species and environmental implications related to wood storage areas. *Water Environ. J. 28*(2), 277-284.

Tao, W., Hall, K.J., Masbough, A., Frankowski, K., Duff, S.J., 2005. Characterization of leachate from a woodwaste pile. *Water Qual. Res. J. Can.* 40, 476–483.

Tollner, E. W., Das, K. C., 2004. Predicting Runoff From A Yard Waste Windrow Composting Pad. *T. ASAE. 47*(6), 1953-1961. doi:10.13031/2013.17808

US Composting Council. 2010. Test methods for the examination of composting and compost. http://compostingcouncil.org/tmecc/

USEPA, 2018. *Advancing Sustainable Materials Management: 2015 Fact Sheet*. Washington, DC: U.S. Environmental Protection Agency, Office of Land and Emergency Management.

van Genuchten, M. Th., 1980. A closed-form equation for predicting the hydraulic conductivity of unsaturated soils. *Soil Sci. Soc. Am. J.* 44(5), 892.

van Genuchten, M. Th., Wierenga, P. J., 1976. Mass transfer studies in sorbing porous media I. Analytical solutions. *Soil Sci. Soc. Am. J. 40*(4), 473.

Vrugt, J. A., 2016. Markov chain Monte Carlo simulation using the DREAM software package: Theory, concepts, and MATLAB implementation. *Environ. Modell. Soft.* 75, 273-316.

Vrugt, J., Bouten, W., Weerts, A., 2001. Information Content of Data for Identifying Soil Hydraulic Parameters from Outflow Experiments. *Soil Science Society of America Journal, 65*(1), 19.

Wilson, B. G., Haralampides, K., Levesque, S., 2004. Stormwater runoff from open windrow composting facilities. *J. Environ. Eng. Sci. 3*(6), 537-540.

Yao, K. Z., Shaw, B. M., Kou, B., Mcauley, K. B., & Bacon, D. W., 2003. Modeling ethylene/butene copolymerization with multi-site catalysts: Parameter estimability and experimental design. *Polym. React. Eng.* 11(3), 563-588.

Zambra, C., Moraga, N., Escudey, M., 2011. Heat and mass transfer in unsaturated porous media: Moisture effects in compost piles self-heating. *Int. J. Heat Mass Tran.* 54(13-14), 2801-2810.

Table 2.1 Setup for the SPM and DPM inferences with DREAM$_{ZS}$. The prior distributions $p(x)$ are given in the notation $N(\mu, \sigma)$, which stands for a univariate normal distribution with mean μ and standard deviation σ. The min and max of the Range column represent the bounds on each parameter's possible proposal space.

	Woodchip Materials			Portland Cement
	Fixed	$p(x)$	Range (min, max)	Fixed Value
θ_s	-	$N(0.70,\ 0.033)$	0.60, 0.80	0.131
$\log(\alpha)$	-	$N(-0.40,\ 0.033)$	-0.50, -0.30	-3.00
$\log(n)$	-	$N(0.25,\ 0.033)$	0.15, 0.35	0.207
$\log(w_2)^{‡}$	-	$N(-1.5,0.330)$	-2.25, -0.30	-
$\log(\alpha_2)^{‡}$	-2.40	-	-	-
$\log(n_2)^{‡}$	0.061	-	-	-
K_s	54	-	-	3.5
l	0.5	-	-	-0.5

‡DPM Parameter only; θ_s: saturated volumetric water content; α and n: fitting parameters in Eq. 3 and Eq. 5; w_2: dual pore partitioning parameter in Eq. 5; α_2 and n_2: fitting parameters in Eq. 5; K_s: saturated hydraulic conductivity; l: tortuosity

Table 2.2 Summary of measurements. The parameters below the dashed line are the fitting parameters in Eq. 7 used to describe the woodchip particle size distributions.

Pile & Woodchip Characteristics			
	L1	R2	F2
Pile mass (kg)	7377	6260	6175
Pile Volume (m^3)	31.96	28.40	30.09
Total Leachate (m^3)	8.33	7.47	6.95
ρ_d (Mg m^{-3})	0.23	0.22	0.21
θ_{init} (m^3 m^{-3})	0.15	0.11	0.11
d_g (±std. dev.; µm)	3476 (±768)	1554 (±380)	1825 (±220)
d_{50} (µm)	2494	963	1170
I_d	9067	2905	3219
k_d	1.50	1.57	1.62

ρ_d: Bulk density; θ_{init}: Initial volumetric water content; d_g: geometric mean woodchip particle diameter; d_{50}: median woodchip particle diameter; I_d and k_d: fitting parameters.

Table 2.3 Estimability rankings for six combinations of SPM and DPM parameters from Subroy *et al.* (2014).

		1		2		3		4		5		6		Mean Rank	Median Rank	Mode Rank
	Parameter	Value	Rank	Value	Rank	Value	Rank	Value	Rank	Value	Rank	Value	Rank			
SPM	θ_s	0.85	2	0.78	2	0.8	2	0.74	2	0.84	2	0.79	2	2	2	2
	α	0.58	3	0.38	4	0.66	4	0.38	3	0.46	4	0.65	3	3.5	3.5	3
	n	1.36	1	1.39	1	1.39	1	1.57	1	1.43	1	1.37	1	1	1	1
	K_s	58	4	64	3	63	3	59	4	66	3	57	4	3.5	3.5	4
DPM	θ_s	0.85	2	0.78	1	0.8	2	0.74	4	0.84	2	0.79	2	2.17	2	2
	α_1	0.83	6	0.39	3	0.65	4	0.4	5	0.65	5	1.75	5	4.67	5	5
	n_1	1.57	1	2.1	4	1.56	1	1.62	1	1.8	1	1.99	4	2	1	1
	K_s	58	7	64	6	63	7	59	6	66	3	57	7	6	6.5	7
	w_2	0.014	4	0.187	7	0.097	5	0.006	2	0.17	4	0.35	3	4.17	4	4
	α_2	0.069	5	0.071	5	0.058	6	0.004	3	0.023	7	0.019	1	4.5	5	5
	n_2	1.15	3	1.12	2	1.32	3	1.16	7	1.4	6	1.13	6	4.5	3	3

θ_s: Saturated volumetric water content; α and n: Fitting parameters in Eq. 3; K_s: Saturated hydraulic conductivity; α_1, n_1, α_2 and n_2: Fitting parameters in Eq. 5; w_2: Dual pore partitioning parameter in Eq. 5

Table 2.4 The *maximum a posteriori* (MAP) estimates and mean ± standard deviation of the posterior distributions (Dist.) of the optimized SPM and DPM water retention parameters for the L1 and R2 piles.

		L1		R2	
	Parameter	MAP	Dist.	MAP	Dist.
SPM	θ_s	0.640	0.66 ±0.03	0.745	0.76 ±0.02
	$log_{10}(\alpha)$	-0.390	-0.36 ±0.03	-0.360	-0.34 ±0.02
	$log_{10}(n)$	0.181	0.19 ±0.01	0.183	0.19 ±0.01
DPM	θ_s	0.653	0.70 ±0.04	0.733	0.72 ±0.05
	$log_{10}(\alpha_1)$	-0.392	-0.40 ±0.04	-0.343	-0.36 ±0.03
	$log_{10}(n_1)$	0.224	0.24 ±0.04	0.212	0.20 ±0.02
	$log_{10}(w_2)$	-1.39	-1.5 ±0.34	-1.02	-1.6 ±0.35

θ_s: Saturated volumetric water content; α and n: Fitting parameter in Eq. 3; α_1 and n_1: Fitting parameters in Eq. 5; w_2: Dual pore partitioning parameter in Eq. 5

Table 2.5 The E_f and $RMSE$ (mean ± standard deviation) for the SPM and DPM models using 100 random posterior samples using all data (All) or a subset that excluded the unexpected measured responses (UR) when significant storms occurred, but no leachate was measured (Fig. 2.2). The R2 optimized parameters for the SPM and DPM were validated in the F2 woodchip pile.

		E_f		$RMSE$ (L/6 hr)	
		All	UR	All	UR
L1	SPM	0.73 ±0.01	0.76 ±0.01	28 ±0.21	26 ±0.27
	DPM	0.72 ±0.06	0.75 ±0.06	29 ±1.0	27 ±0.94
R2	SPM	0.80 ±0.01	-	23 ±0.25	-
	DPM	0.80 ±0.03	-	24 ±0.50	-
F2	SPM	0.62 ± 0.01	0.72 ±0.01	33 ±0.42	26 ±0.20
	SPM†	0.62 ±0.01	0.73 ±0.02	33 ±0.66	26 ±0.35
	DPM	0.63 ±0.01	0.75 ±0.02	34 ±0.71	26 ±0.36
	DPM†	0.63 ±0.01	0.76 ±0.02	24 ±1.1	26 ±0.52

† Combined L1+R2 multivariate distributions were used

E_f: Nash-Sutcliffe efficiency Index; $RMSE$: Root mean square error

Figure 2.1 (A) Diagram of the experimental setup and leachate collection system; (B) A picture of the experimental setup; (C) A discretized three-dimensional HYDRUS domain based on the L1 pile geometry. The arrows show how precipitation (P) and evaporation (E) fluxes occur from the topmost surfaces, while leachate (L) fluxes leave by a seepage face designated as the bottom surface of the swale.

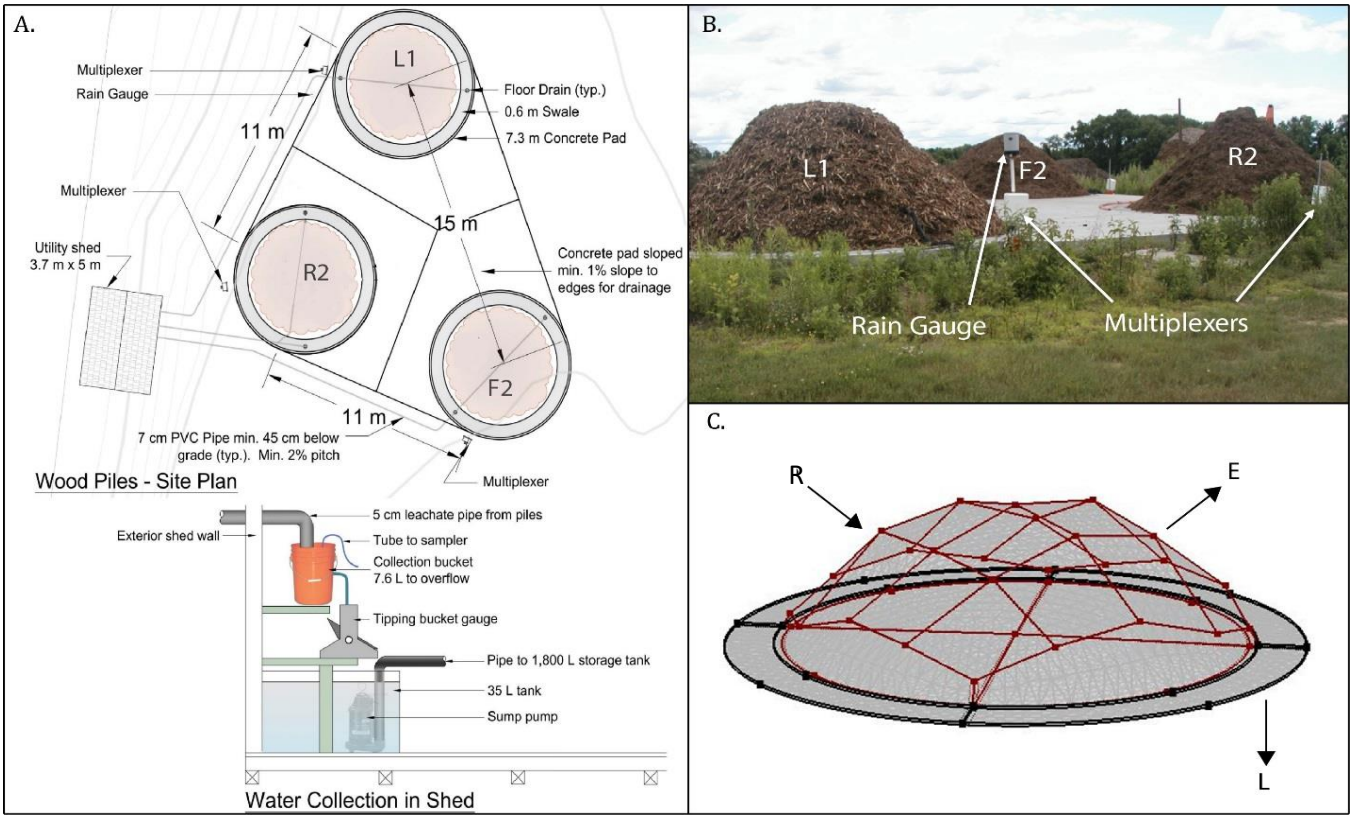

Figure 2.2 Cumulative leachate volumes collected from the three experimental piles compared to measurements of hourly precipitation from the Mansfield, NJ weather station.

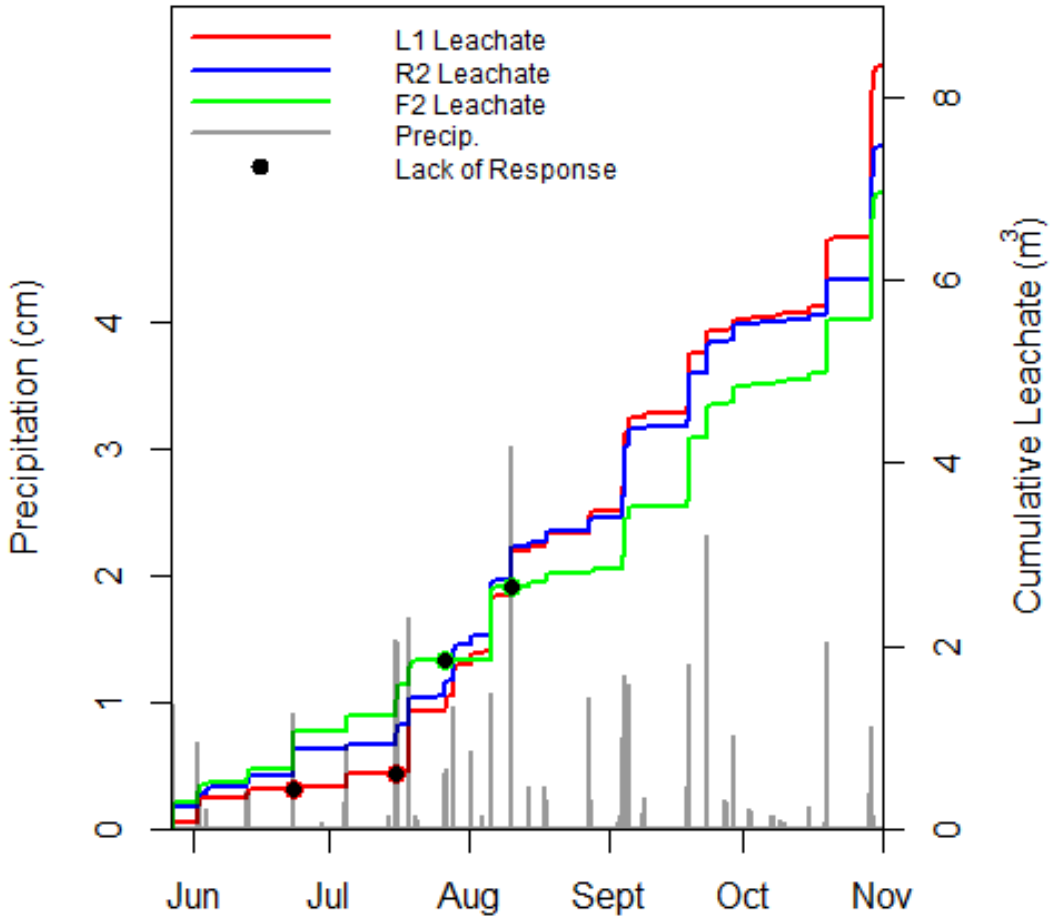

Figure 2.3 Results of subtracting the posterior distributions of the twice ground woodchip pile R2 from the once ground woodchip pile L1 (contrast=L1-R2). The result of each parameter contrast is a density distribution (shaded in color) with an IQR denoted by the dashed vertical lines. The solid line indicates the position of a contrast equal to zero.

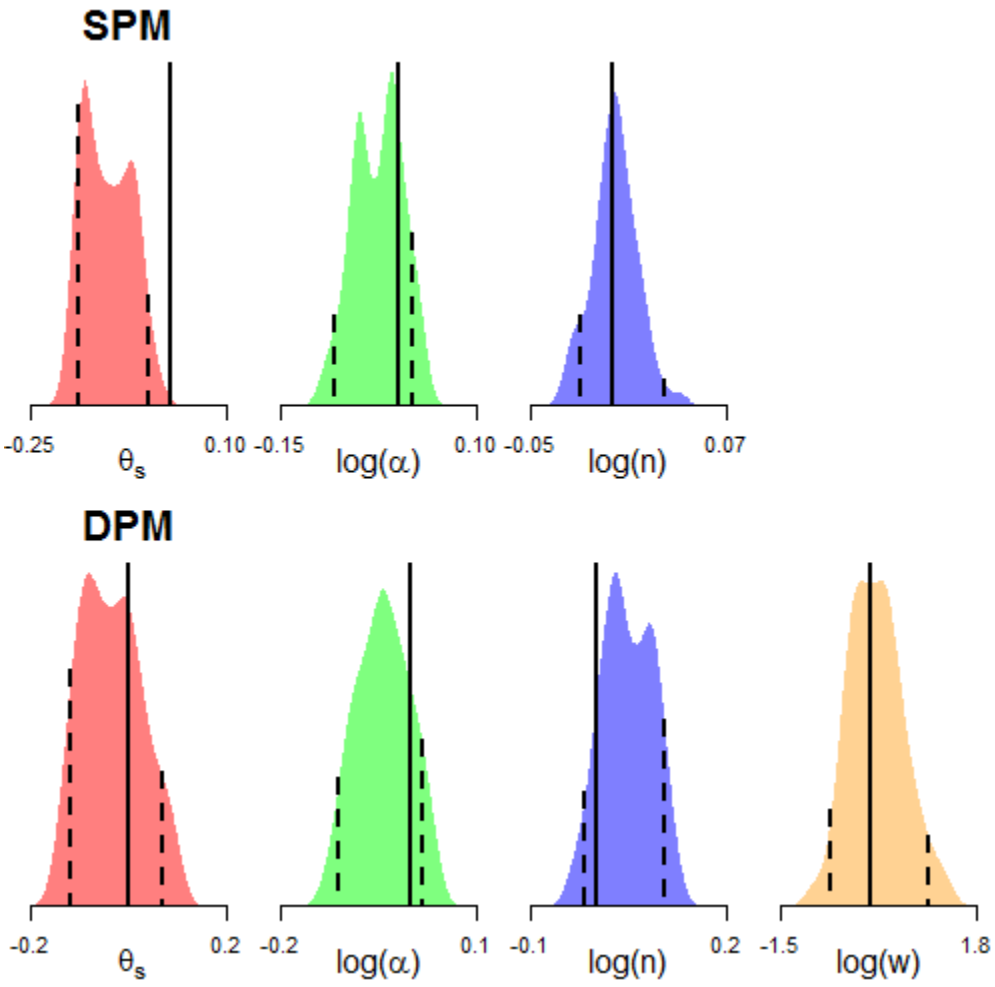

Figure 2.4 Correlation scatter plots and density distributions (shaded in color) for the hydraulic parameters of the DPM model after combining the posterior distributions for the L1 and R2 piles. The normal distribution indicated by the solid line represents that parameter's prior probability distribution (Table 2.1). The dashed and solid lines on the x-axis represent the *maximum a posteriori* (MAP) parameter estimates for the L1 and R2 piles, respectively (Table 2.4). The straight lines drawn through the scatter plots are the best fit line and the titles are the parameter's correlation/covariance.

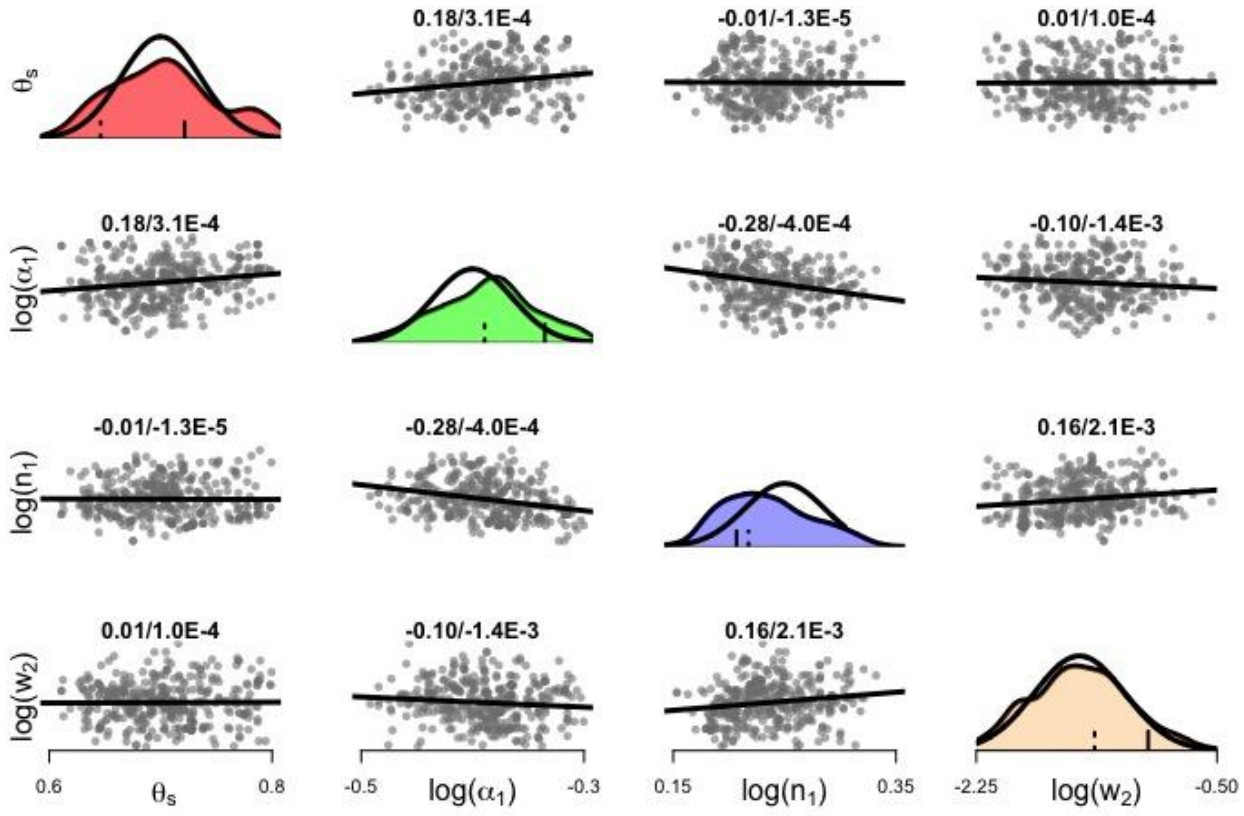

Figure 2.5 Cumulative measured leachate volume compared with the 95% interval of confidence predicted by the SPM and DPM water retention models (not including the storms with lacks of leachate responses- Fig. 2.2). The 2.5th and 97.5th percentiles were calculated based on the simulation results of N=100 posterior samples. To predict leachate from the F2 pile, the posterior for the R2 hydraulic parameter sets (Table 2.4) were used.

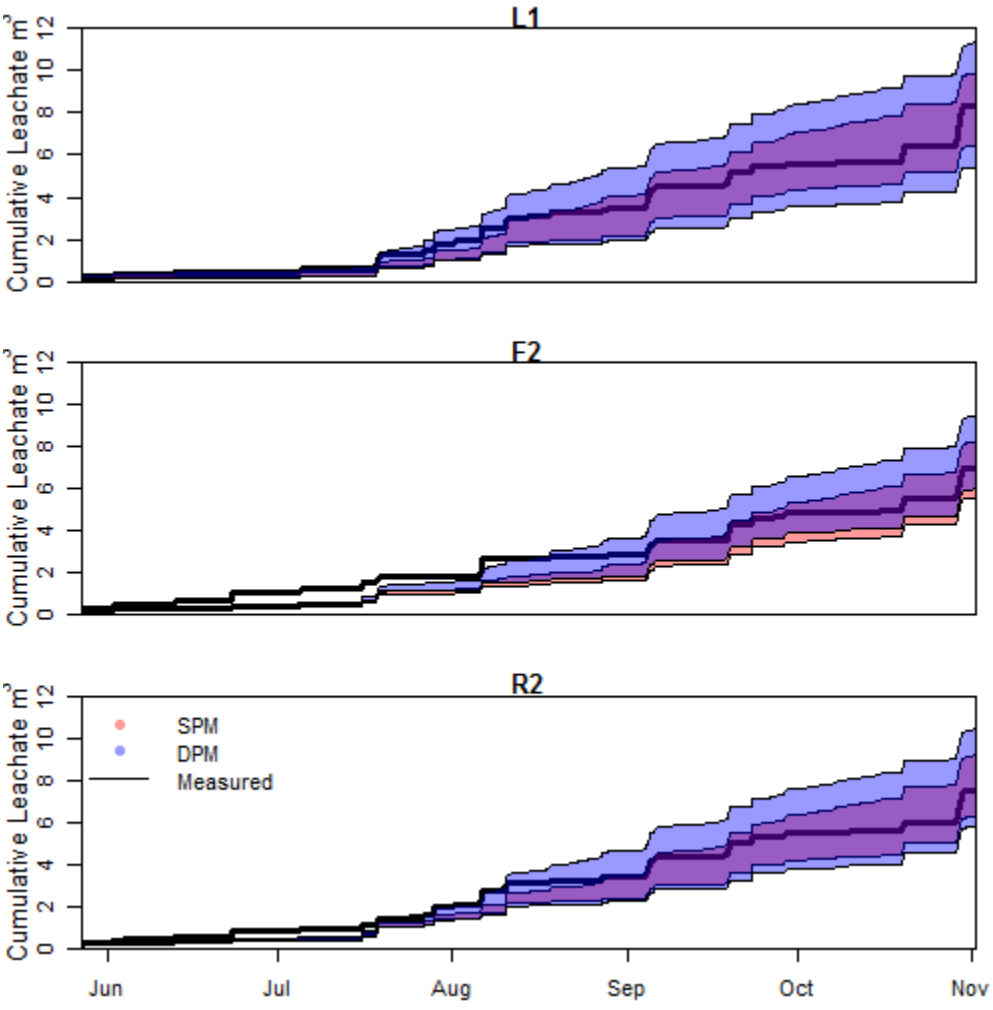

Figure 2.6 HYDRUS predictions from the R2 optimizations (N=100) versus measurements of 6-hr leachate for the F2 woodchip pile. The vertical lines denote the interval between the minimum and maximum leachate prediction. The solid black line represents a perfect 1:1 correlation, while SPM-Cor and DPM-Cor are the best fit linear correlation for each water retention model.

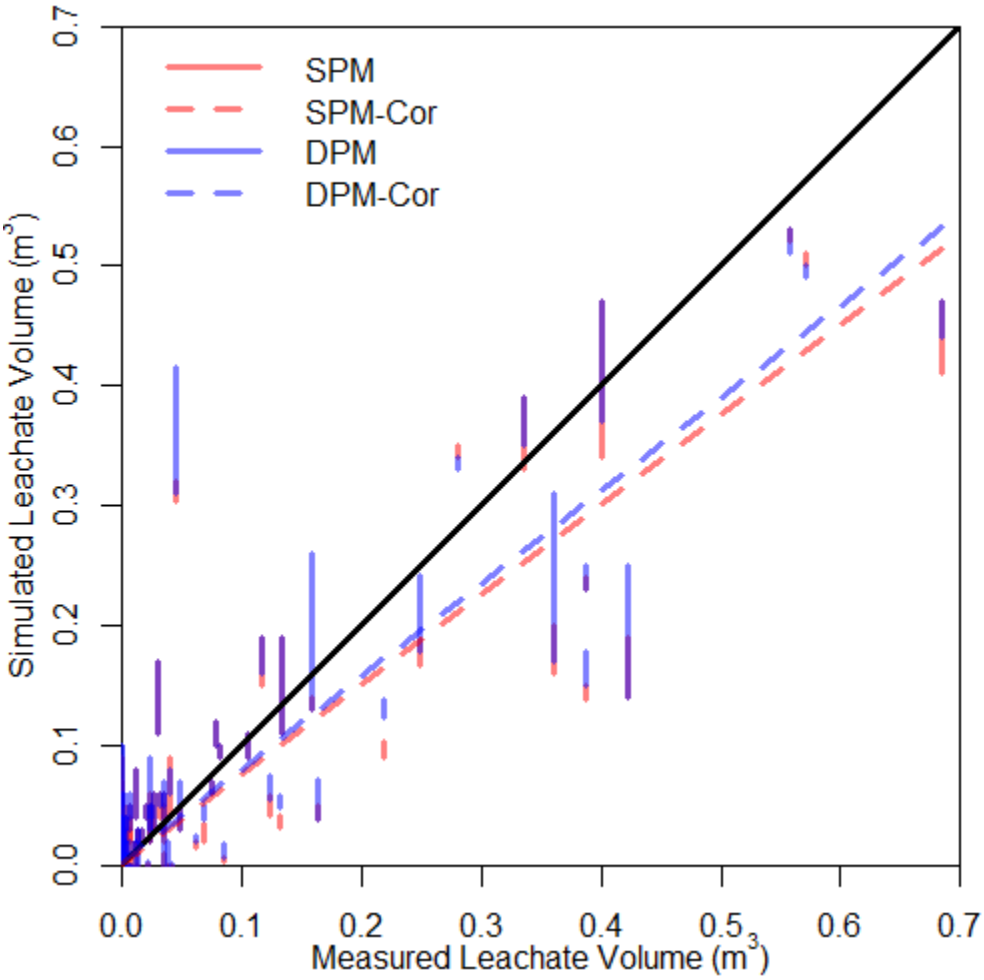

Figure 2.7 Residuals between predicted and measured leachate broken down into small (Sm; green), medium (Med; blue) and large (Lrg; red) 6-hr storm events.

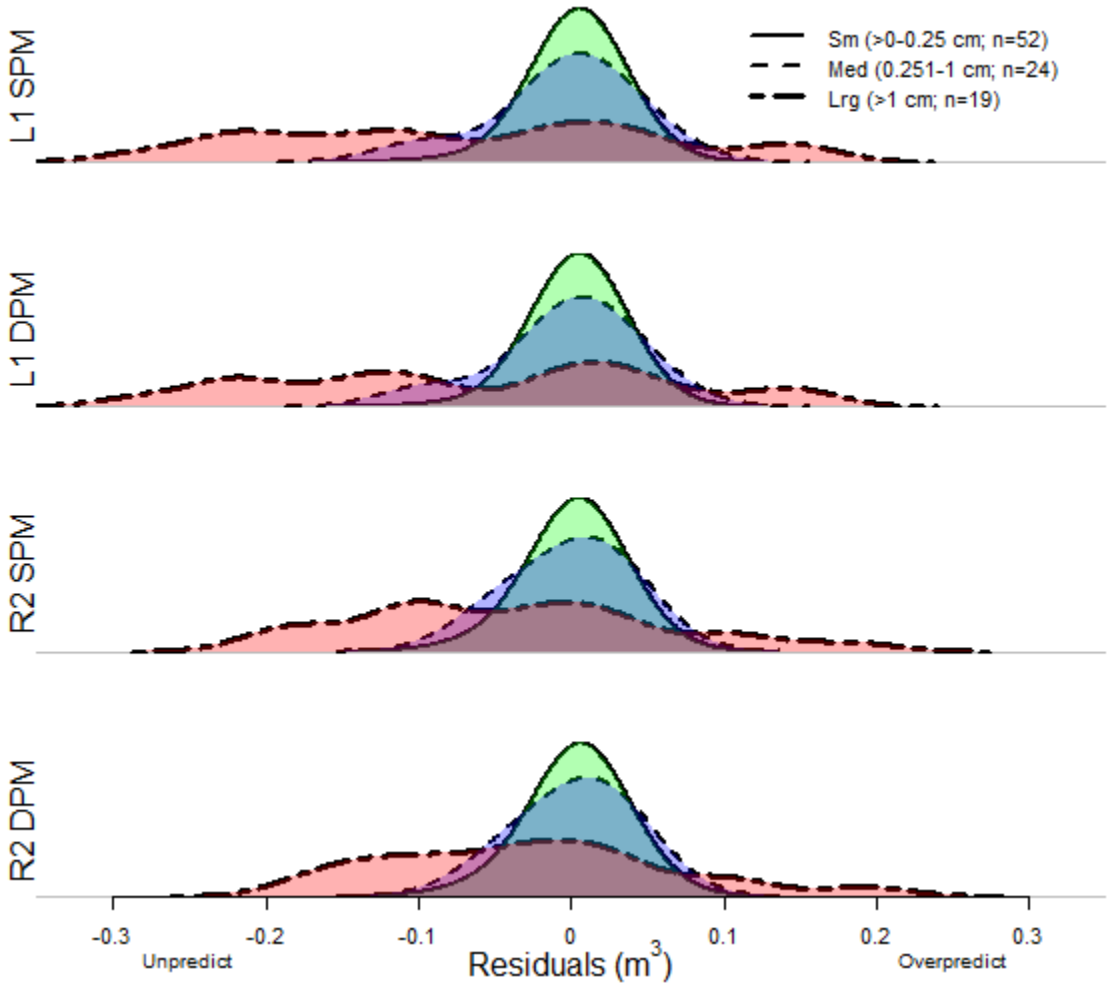

3. Dielectric Permittivity-Water Content Relationships in Woodchips: Particle Size and Temperature Effects

Material in this chapter has been published previously as:

Amato, M. T., Subroy, V., Giménez, D., Strom, P. F., Krogmann, U., 2019. Dielectric permittivity-water content relationships in woodchips: Particle size and temperature effects. *J. Hydrol. 572*, 251-260.

3.1 Abstract

Information on the amount of water held by ground woodchips in the field is needed to assess environmental risks when they are kept in stockpiles or for inferring their efficiency as denitrifying bioreactors. Reflectometry is a widely used method for estimating volumetric water content (θ) in permeable media, but material-specific calibration functions should be developed. This study aimed at developing relationships between the bulk dielectric permittivity ($\sqrt{\varepsilon_b}$) and θ in woodchips considering their particle size distribution (PSD), temperature (T) and the dielectric permittivity of the dry material plus air ($\sqrt{\varepsilon_{sa}}$). The $\sqrt{\varepsilon_b}$ of fine, medium and coarse PSDs were measured with CS616-L water content reflectometers up to θ of 0.83 cm^3/cm^3 and at T (° C) of 10°, 24°, 37°, 55° and 70°. Calibration equations were developed using a multivariate power law function fitted to the data with a hierarchical Bayesian inference procedure. The best fit (R^2=0.96; $RMSE$=0.04 cm^3/cm^3) was obtained for the fine PSD ($\sqrt{\varepsilon_{sa}}$~1.09); while medium ($\sqrt{\varepsilon_{sa}}$~1.09) and coarse ($\sqrt{\varepsilon_{sa}}$~1.03) PSDs were more influenced by T and the presence of large air voids (R^2~0.92; $RMSE$~0.06 cm^3/cm^3). A modified calibration equation independent of PSD ($\sqrt{\varepsilon_{sa}}$=1) reduced only slightly the goodness-of-fit (R^2=0.90; $RMSE$=0.07 cm^3/cm^3). The equations developed in this study are well suited for field applications as they cover a wider range

of θ than previously published functions and they are applicable within the range of T found in field applications.

3.2 Introduction

Monitoring water content within ground woody biomass (woodchips) is important for practitioners in the agricultural, energy, forestry and waste management industries (Afzal *et al.*, 2009; Fenton *et al.*, 2014; Kannepalli *et al.*, 2016). For instance, open stockpiles of woodchips present potential environmental hazards through their ability to self-ignite (Li *et al.*, 2006) and generate harmful leachate during precipitation and irrigation events (Hedmark and Scholz, 2008; Tao *et al.*, 2005). There is also an economic incentive to maintain the quality of the stockpiled woodchip materials by keeping the piles sufficiently dry (Lenz *et al.*, 2015; Lin and Pan, 2015). Additionally, woodchip's are popularly used as filling medium in denitrifying bioreactors (Addy *et al.*, 2016; Jitka *et al.*, 2017). Their ability to maintain high hydraulic conductivity (van Driel *et al.* 2006), which is a function of their water content (Subroy *et al.* 2014), is key to their efficiency and long-term operation.

Time domain reflectometry (TDR) is a widely used method for measuring spatiotemporal variations in water content due to its accuracy, practicality and ability to be automated (Jones *et al.*, 2002). This technique computes the apparent bulk dielectric permittivity (ε_b), which is defined as the squared ratio of the propagation velocity of an electromagnetic (EM) pulse in vacuum relative to the medium in which the waveguide is embedded (Jones *et al.*, 2002). The dielectric permittivity of oven dry wood material (ε_s) with density between 0.1-1.5 g/cm^3 varies from 1.3 to 4.5 when measured at a frequency of 100 MHz, which is more than an order of magnitude smaller than that of pure deionized water (ε_w~ 80). This contrast is used to detect water content by measuring the bulk medium's dielectric permittivity (Topp *et al.*, 1980; Torgovnikov, 1993).

Water content reflectometers, such as the CS616-L model manufactured by Campbell Scientific, Inc., have been promoted as a cost-effective alternative to TDR instruments as they are durable for long-term usage in the field and do not require a separate waveform analysis to compute ε_b. Instead, reflectometers are internally programmed to record the number of EM pulse reflections per second, which is proportional to $\sqrt{\varepsilon_b}$ and, through calibration, to the volumetric water content θ (Kelleners *et al.*, 2005). However, because water content reflectometers operate at a lower frequency (~175 MHz) than traditional TDR instruments (~ 500-1000 MHz) they are more sensitive to surrounding environmental conditions, such as temperature (Kapilaratne and Lu, 2017), as well as characteristics of the material itself, such as porosity, composition and specific surface area (Roth *et al.*, 1990; Malicki *et al.*, 1996; Or and Wraith, 1990; Skierucha *et al.*, 2012). As a consequence, material-specific relationships between $\sqrt{\varepsilon_b}$ and θ that consider the effect of temperature should be developed when using the CS616-L probe (Quinones *et al.*, 2003; Logsdon, 2009).

Bulk dielectric permittivity is commonly related to water content using the third-order polynomial relationship proposed by Topp *et al.* (1980) or the linearized equation proposed by Ledieu *et al.* (1986). These and other empirical relationships (Table 3.1) have been calibrated to measure stem water contents in whole wood materials like tree trunks, logs and timber (Constantz and Murphy, 1990; Gray and Spies, 1995; Wullschleger *et al.*, 1996; Malicki *et al.*, 1998; Nadler *et al.* 2003; Hernández-Santana and Martínez-Fernández, 2008; Schimleck *et al.*, 2011; Dahlen *et al.*, 2015). Similar relationships in ground woody materials like woodchips, tree tops and saw dust are less documented (Paz *et al.*, 2006; Paz *et al.*, 2010; Mendel *et al.*, 2016). Paz *et al.* (2010) proposed using mixing models to predict water content in ground woody materials (Table 3.1). Mixing models are physically sounder than empirical equations, but require data on the volumetric portions, geometric configurations and dielectric properties for each of the constituents comprising the bulk mixture (Sihvola and Kong, 1988; Roth *et al.*,

1990). The geometric configuration of the constituents is difficult to know *a priori* and it is typically obtained by fitting the model to data (*e.g.* Paz *et al.* (2010)).

The scope of this study was to calibrate a mathematical relationship between $\sqrt{\varepsilon_b}$ and θ as measured by a CS616-L water content reflectometer in mixtures of woodchip particles of various sizes and temperatures between 10° and 70° C. This corresponds roughly to the range of temperatures measured in controlled experimental woodchip stockpiles (Kannepalli, 2014) and also covers standard temperature conditions within agricultural denitrifying beds (~10° C; Addy *et al.* 2016). The objectives were to (1) determine if particle size and/or temperature were significant factors for modeling the $\theta\ vs\ \sqrt{\varepsilon_b}$ relationship in woodchip mixtures and (2) calibrate $\theta\ vs\ \sqrt{\varepsilon_b}$ functions taking into account any significant factors. A hierarchical Bayesian inference framework was used such that the uncertainty of the calibration function and measurements are accounted for during the parameter inference process.

3.3 Materials and Methods

The $\theta\ vs\ \sqrt{\varepsilon_b}$ relationship was measured in woodchip samples with three different particle size distributions at five different temperatures: 10° C, 24° C, 37° C, 55° C and 70° C. The samples used in the experiments were selected from a subset of woodchip mixture samples, previously characterized by Subroy *et al.* (2014). Air-dried samples were represented by their geometric mean diameter (d_g) calculated as

$$d_g = \prod_{i=0}^{n} d_{gi}^{fi} \tag{1}$$

where d_{gi} is the geometric mean between the ith and $(i+1)^{th}$ sieve openings, f_i is the mass fraction that is retained on the ith sieve and n is the number of sieves. A set of 10 US Standard sieves with openings (mm) of 25.40, 19.05, 9.53, 5.66, 2.83, 1.41, 0.59, 0.30, 0.15, and 0.06 were used. The lower (i=0) and upper bound ($(i+1)^{th}$=11) to calculate d_{gi} for the smallest and largest sieve diameters were

assumed to be 10^{-3} and 50.8 mm, respectively. Samples selected for calibration had d_g (± std. dev.) values of 2255 (±260) µm, 4402 (±1852) µm and 8130 (±1354) µm (Fig. 3.1), and are representative of woodchip mixtures with a predominance of fine-, medium-, and coarse-sized woodchip particles, respectively.

3.3.1 Experiment

Woodchip samples were packed into rectangular polypropylene containers that were 32.5 cm long, 15 cm wide and had a height of 10 cm. Each container had five apertures on the side that were distributed uniformly from the base to the top of the container. Male luer fittings 0.16 cm in I.D. were attached to each aperture, which served as both water delivery and drainage ports (Fig. 3.2). Filter paper was applied over the ports on the inside surface of the container to prevent them from clogging during drainage and to facilitate a uniform dispersion of water during saturation. A CS616-L water content reflectometer and a 109-L thermistor (both Campbell Scientific, Inc., Logan, UT, USA) were inserted horizontally into the container at a height of 4 cm through openings made in the plastic (Fig. 3.2). Air-dried woodchip material was packed incrementally around the waveguides to a dry bulk density of 0.245 ±0.049 g/cm^3, which is similar to that measured in experimental woodchip stockpiles (Kannepalli, 2014).

A run consisted of a saturation experiment followed by a drainage/drying experiment for each of the three woodchip samples. Each run was performed at the five temperatures starting with the lowest temperature of 10° C. Runs conducted at temperatures between 10° C and 40° C were carried out in a growth chamber (GC15, Environmental Growth Chambers, Chagrin Falls, OH), while those performed at 55° C and 70° C were done in an oven (Model 800, Memmert GmbH + Co. KG, Schwabach, DE). Before each run started at a particular temperature, the containers of packed material along with the reservoir of deionized water used to saturate the samples were equilibrated at that desired

temperature overnight. Containers were covered with lids during saturation experiments to reduce evaporative losses; however, the lids did not seal air tight. At the beginning of the saturation experiment all three samples, one per container, were simultaneously wetted from the reservoir through a syringe pump equipped with six 3-ml capacity syringes (Soil Measurement Systems, Tucson, AZ, USA) that delivered water at an average rate of 19.4 mL/min with an average standard deviation of 1.4 mL/min. Water from two syringes was directed into a single tube connected to a five-way manifold. Each line of the manifold was connected to one of the five ports along the side of the containers through a one-way valve that prevented backflow. Each container was placed on a balance (XS 32001L, Mettler Toledo, Columbus, OH, USA) with precision of 0.1 g to measure the amount of water being delivered into the samples (Fig. 3.2). Readings from the balances were collected every minute using the Lab X software (Mettler Toledo), while data from the probes were collected simultaneously using a CR1000 data logger (Campbell Scientific, Inc.).

A saturation experiment ended when the box was filled and the output from the CS616-L sensor had stabilized. At this time, the syringe pump was turned off, the lids were removed, the manifold was disconnected and the water in the samples was allowed to drain by gravity and simultaneously evaporate. The decreasing weights of the open containers as well as the corresponding CS616-L and 109-L probe readings were recorded every minute for the first 2 hours and every 15 or 30 minutes after that. After gravity-driven drainage had ceased, the samples were allowed to dry by evaporation at near constant temperature for the next 2-3 days before starting a new run with the same material at the next higher temperature.

At 55° C and 70° C, the calibration set-up had to be modified because the balances and the syringe pump could not be placed inside the drying oven. The weight of water added to the container was determined by weighing the container before and after saturation and dividing the added weight of water equally across the saturation time. During free drainage at 55° C and 70° C, water draining from

the samples was routed through tubing attached to the ports, which emptied into separate containers placed on the balances outside of the drying oven. Free drainage ended once water ceased to flow out by gravity. At this time, the lids were removed and water from the packed material was allowed to evaporate. The packed containers were then periodically weighed over the next 5-6 days. After a run had been recorded at each temperature and for each sample, the containers were re-packed with a new subsample of the same material and the entire procedure was repeated in order to obtain duplicate data sets.

3.3.2 Determination of the Water Content

The effective volume sensed by the CS616-L water content reflectometer was smaller and had a different shape than the container. Thus, the size and shape of this volume had to be estimated to properly account for the fraction of the total water actually within the sensor's range at any given time. Perpendicular to the direction of the waveguides, the sensed area was assumed to have the shape of an ellipse (Ferré *et al.*, 2002; Germann, 2017). Following Baker and Lascano (1989), the three-dimensional shape of the effective volume was a half-ellipsoid cut on its vertical axis at the point of insertion of the waveguides into the sensor head (Fig. 3.3).

The effective volume considered had a constant length of 30 cm (the length of the probes) and a constant width of 15 cm (the width of the container). The height dimension of the volume changed each run and was computed from the range of the water level when the sensors initially responded to changes in water content to when they ceased to respond. The response of the sensor during saturating and free drainage experiments followed a symmetrical sigmoidal relationship (data not shown) similar to the one reported in Germann (2017). This implies that the shape of the response was the same at the early and late stages of saturation/drainage, and that the effective sensing volume did not change over time.

As a result of the ellipsoidal shape of the effective volume, equal filling/draining rates resulted in larger changes in the readings made by the CS616-L as the level of water approached the waveguides (Fig. 3.3). This is because changes in water content closer to the waveguide occurred within a larger portion of the effective volume, whereas the opposite is true with changes in water content further from the waveguide. The ratio of the effective volume filled over the total volume of the container that was filled was used to correct for the amount of water inside the effective volume. This correction method was used for saturating experiments and the free drainage portion of the draining experiments.

For the evaporative drying part of the draining experiments, changes in water content were assumed to be uniform throughout the container because the relationship between the sensor's output and mass of the drying woodchips was linear (data not shown). A similar assumption is used to interpret evaporation from soils (Schindler *et al.*, 2010) and leads to a linear decrease of water from the bottom of the container to the evaporating surface. Since sensors were placed in the middle of that vertical span, measurements are representative of the woodchip's average water content during evaporation.

3.3.3 Apparent Bulk Dielectric Permittivity

The output of the CS616-L water content reflectometer is period P (T), which is inversely related to the number of pulse reflections recorded per second f_r (T^{-1}), and can be used to compute the travel time t (T) by the following relationship (Campbell and Anderson, 1998)

$$t = \frac{2}{f_r} = \frac{P}{S_f} \tag{2}$$

where S_f is a scaling factor (-) equal to 1024 for the CS616 reflectometer model (Logsdon, 2009). Travel time t is related to $\sqrt{\varepsilon_b}$ as (Kelleners *et al.*, 2005)

$$\sqrt{\varepsilon_b} = \frac{(t - 2t_d)c}{4L_a} \quad (3)$$

where t_d is the delay time between the step pulse voltages emitted by the reflectometer and is approximately equal to 5.4 x 10^{-9} s, c is the speed of light (3.0 x 10^8 m/s) and L_a is the apparent length of the waveguide, which is not equal to its physical length (30 cm), but is instead taken to be 26 cm (Logsdon, 2009). The rationale for converting P to $\sqrt{\varepsilon_b}$ was to allow for comparisons with other TDR studies and their reported calibration relationships with θ.

3.3.4 Inference

Bayesian inference methods were applied to address uncertainty arising from experimental procedures, hypothesis testing and the selection of a calibration function. Bayesian methods assign probabilistic distributions to the parameters being inferred and then update them based on observational data (Gelman *et al.*, 2015). In this work, the parameters were conditioned with measurements of $\sqrt{\varepsilon_b}$ and θ in a normal likelihood function such that the maximum *a posteriori* estimates for the parameters could similarly be attained with a least squares regression. The mean of the normal likelihood function was set equal to θ predicted by a given calibration function. The standard deviation of the normal likelihood function, which is related to the root mean square error ($RMSE$) of the calibration function, was inferred along with the unknown parameters of the calibration function.

A hierarchical Bayesian inference model was used to obtain posterior probability distributions for all of the inferred parameters of a calibration function that translated the experimental data from $\sqrt{\varepsilon_b}$ to θ for either a specific particle size distribution or temperature (group-level) and for all data (overall-level) simultaneously (Gelman *et al.*, 2015). The parameter values were assumed to be unknown at all levels in the hierarchical model, therefore weakly informative prior distributions were assigned to give more weight on the data during the inference procedure. Group-level parameters subjected to

inference were pooled under common normal prior distributions, each defined by an unknown common mean and unknown common variance (hyperparameters in Bayesian terminology, Gelman *et al.* (2015)). The hyperparameters, which defined the calibration function at the overall-level, were also unknown and were assigned their own prior distributions (hyperpriors). The common mean was assigned a flat normal hyperprior distribution with a mean of 0 and variance of 10,000. The common variance was assigned a flat uniform hyperprior distribution between 0.0001 and 10,000. The $RMSE$ was inferred independently for all groups in the hierarchical model and in each case it was assigned a flat gamma distribution with both shape parameters equal to 0.00001 (Gelman *et al.*, 2015).

The R package 'rjags' was used to identify the posterior distribution for all of the unknown parameters (Plummer, 2016). Four MCMC chains were each programmed to run for a burn-in period of 10,000 generations until all four chains converged for each parameter. Convergence was diagnosed with the Gelman and Rubin (1992) scale reduction statistic $\hat{R}$ as calculated by the CODA package (Plummer *et al.*, 2006). Chains were considered converged when $\hat{R}$ stabilized below 1.05, after which it was assumed that any subsequent MCMC sample was to be accepted as a member of the posterior distribution. In total, 40,000 independent samples from the posterior distribution were drawn (10,000 from each of the four chains) for each parameter and used for hypothesis testing and uncertainty analyses.

The posterior distribution of the inferred parameters were summarized by their 95% credible interval (Cr. I.), which is a continuous range of values that has a 95% probability of containing the "true" parameter value in it. The 95% Cr. I. for the group-level parameters were compared by contrast (subtracting one from the other), in order to determine significant differences between temperature and particle size groups separately. If the 95% Cr. I. for a given contrast was overlapping (contained zero) then the effects between the two groups could be considered insignificant (Gelman and Hill, 2016). Multiple comparisons between particle size and temperature groups are acceptable within

Bayesian hierarchical models because all of the parameters are obtained simultaneously from common prior distributions (partial-pooling) (Gelman *et al.*, 2012). The 95% Cr. I.'s for the inferred parameters of the calibration functions were used to identify a 95% Cr. I. for θ given a measurement of $\sqrt{\varepsilon_b}$. The 95% prediction interval (P.I.) was also identified for θ, which is an interval that takes into account the uncertainty of the measurements, by considering the 40,000 posterior samples of the $RMSE$. The P.I. for θ is wider than the Cr.I. for θ, although it should be noted that both intervals are centered around the same conditional mean value of θ.

3.3.5 Calibration

Two separate nonlinear regressions were set up using the hierarchical Bayesian formalism to individually assess the effects of particle size and temperature on the $\theta \; vs \; \sqrt{\varepsilon_b}$ relationship. The equation used in this hierarchical regression was

$$\theta_j = \alpha_j(\sqrt{\varepsilon_{b,j}} - \sqrt{\varepsilon_{sa,j}})^{\beta_j} \tag{4}$$

where α_j and β_j are empirical fitting parameters of the jth group where j=3 for particle size (fine, medium, and coarse) or j=5 for temperature (10° C, 24° C, 37° C, 55° C and 70° C). The dielectric permittivity of the dry material plus air ($\sqrt{\varepsilon_{sa}}$) was measured for each particle size when the material was air-dried (before the start of the 10° C run). These values were subtracted from $\sqrt{\varepsilon_b}$ to force the regressions through the physically determined origin (*i.e.,* when θ=0 cm^3/cm^3 then $\sqrt{\varepsilon_b}$=$\sqrt{\varepsilon_{sa}}$). This assumes $\sqrt{\varepsilon_{sa}}$ is invariant to changes in temperature; because the increase in ε_s with increasing temperature is minor enough that the effect can be neglected (Torgovnikov, 1993).

Once the effects of particle size and temperature had been analyzed using the contrast method described in section 3.3.4, a power law function of the form

$$\theta_j = \left[\alpha_j(\sqrt{\varepsilon_{b,j}} - \sqrt{\varepsilon_{sa,j}})^{\beta_{1,j}}\right] \cdot T^{\beta_{2,j}} \quad (5)$$

was calibrated for each particle size group using a hierarchical multiple nonlinear regression with two continuous covariates: $\sqrt{\varepsilon_b}$ and temperature T (° C). A set of α, β_1 and β_2 parameters were inferred for each particle size group (group-level) and for all data (overall-level), as well as the $RMSE$ for each group (15 total parameters).

Equation 5 was simplified by pooling the data and assuming $\sqrt{\varepsilon_{sa}} = 1$, making it independent of particle size

$$\theta = \left[\alpha(\sqrt{\varepsilon_b} - 1)^{\beta_1}\right] \cdot T^{\beta_2} \quad (6)$$

After applying this modification, the posterior parameter estimates were obtained in a simpler non-hierarchical Bayesian model, which had four unknown parameters: α, β_1 and β_2 and the $RMSE$.

3.3.6 Validation

Three measurements of θ and $\sqrt{\varepsilon_b}$ were made at target water contents of 0.2, 0.4 and 0.6 cm^3/cm^3 for each particle size at room temperature by thoroughly mixing known masses of water and woodchips and packing the mix around the waveguide of the CS616-L sensor. In addition, field measurements were acquired from an experimental woodchip pile comprised of finely ground woodchip materials (d_g=1554 µm) that was instrumented with multiple CS616-L water content reflectometers and 109-L temperature probes placed at different locations within the pile (Kannepalli, 2014). At the end of a six-month field experiment three samples of woodchips were taken in close proximity to each of 13 probes. In all cases, the volumetric water content was determined by the gravimetric method and the bulk density of the material. Because the three measurements at a given location within the pile were always in close agreement with one another, the average between them was used in the validation. The root mean square deviation ($RMSD$: square root of the sum of the squared residuals divided by the

number of samples), and the percent relative difference (bias: average residual divided by the average measured value of θ), were used as metrics to assess deviations between predictions and the validation data.

3.4 Results and Discussion

Experiments conducted at the five temperatures yielded a wide range of $\theta \; vs \; \sqrt{\varepsilon_b}$ measurements that were not adequately fit by the temperature-independent functions found throughout the literature (Fig. 3.4; Table 3.1). The majority of these functions were developed with TDR measurements taken in whole wood, which usually has a greater density and holds less water than ground wood materials. The linearized function calibrated by Gray and Spies (1995) for use in decaying logs of wood with similar porosity to woodchips (>0.7 cm^3/cm^3, Kannepalli, 2014) closely followed the trend of the experimental data collected in this study (Fig. 3.4). The power law (Roth et al, 1990) and Maxwell-Garnett (Sihvola and Kong, 1988) mixing models as used by Paz *et al.* (2010) were the only functions that were calibrated specifically for use in comminuted wood materials. Their predictions fall within the range of measured values, but are restricted to the θ interval used in their development (~0.08-0.3 cm^3/cm^3).

The experimental design in this study allowed measurements to be made over almost the entire range of possible water contents for a woodchip mixture. This would have been difficult to achieve had the highly porous woodchip samples been mixed and measured separately with the gravimetric method. This is particularly true for measurements taken close to saturation, as water within the large inter-particle pores would be preferentially distributed towards the bottom of the container. Since the gravimetric method assumes a homogenous water content, this would then lead to an under or overestimation of $\sqrt{\varepsilon_b}$ depending on the position of the waveguide relative to the saturated region in the container. The drawback of the experimental design, however, was that the sensor's effective

volume needed to be calculated for each individual experiment in order to accurately compute θ and relate it to measurements of $\sqrt{\varepsilon_b}$. The vertical axis of the effective volume decreased with particle size (Table 3.2), probably because coarse woodchip mixtures had a sharp wetting/drying front that could only be sensed when in close proximity to the waveguides (Fig. 3.3). On the contrary, capillary forces in fine particle mixtures created a diffuse wetting/drying front, ultimately causing the sensor to react sooner and more gradually than in the coarse mixture (Fig. 3.3). The effective volume was also determined to be smaller in saturation experiments when the woodchips started at a drier condition than during draining experiments (Table 3.2), likely because of greater sensitivity of the sensor when water, instead of air, is the continuous phase (Baker and Lascano, 1989; Ferré *et al.*, 1996), which was the case during draining experiments.

3.4.1 Particle Size and Temperature Effects

The 95% Cr. I. for the parameter contrasts of Eq. 4 provide an indication of the similarity between the posterior distributions of the two groups compared. If the Cr. I. of a contrast contains 0, it is likely that the "true" value for that parameter is the same for both groups. In contrast, if the Cr. I. does not contain 0, then it is fair to conclude that the two groups are significantly different from one another. How the two groups differ can be gauged by the sign (positive or negative) and magnitude (distance from zero) of the 95% Cr. I. for that contrast (Gelman and Hill, 2016). Since none of the 95% Cr. I. for the contrasts between the inferred parameters of Eq. 4 contained 0, temperature and particle size were both deemed significant for modeling the $\theta\ vs\ \sqrt{\varepsilon_b}$ relationship for woodchip materials (Fig. 3.5). Accordingly, particle size was considered a categorical covariate, while temperature was included as a continuous covariate in the calibration function (Eq. 5).

Contrasts of the 95% Cr. I. for the parameters of Eq. 4 show that the $\theta\ vs\ \sqrt{\varepsilon_b}$ relationship was most similar between the medium and coarse woodchip mixtures as they were closest to zero, while the

opposite is true for contrasts between the fine and coarse mixtures (Fig. 3.5A). Malicki *et al.* (1996) used bulk density to account for differences in the $\theta\ vs\ \sqrt{\varepsilon_b}$ relationship in porous materials with different particle sizes. In this study, the bulk density values of the woodchip mixtures were virtually the same (Subroy *et al.*, 2014), thus a more probable explanation for these observed differences is how the woodchip particles and their pore network are spatially arranged in relation to the orientation of the EM field (Ansoult *et al.*, 1985; Roth *et al.*, 1990; Jones and Or, 2002). For fine woodchip mixtures, the pore network contains smaller pores that are likely to lead to a more continuous water phase that transmits the EM pulse with less interference from components with low dielectric permittivity, such as solid wood or air. When this is the case, the $\theta\ vs\ \sqrt{\varepsilon_b}$ relationship tends to be linear. In contrast, coarse woodchip mixtures have a more disconnected water phase caused by interferences with large woodchip particles or air voids, resulting in a nonlinear $\theta\ vs\ \sqrt{\varepsilon_b}$ relationship.

Another reason for the observed differences between particle size groups is that insufficient contact between the waveguides and coarse woodchips affected the reproducibility of the measurements. This is evidenced by the increase in the mean $RMSE$ from Eq. 4 (computed from the 40,000 samples in the posterior distribution) for the fine (0.04 cm^3/cm^3), medium (0.06 cm^3/cm^3), and coarse (0.07 cm^3/cm^3) woodchip mixtures (data not shown). Notice that the mean $RMSE$ values for the medium and coarse woodchips are most similar to each other and so are their 95% Cr. I.'s for their inferred parameters (Fig. 3.5A).

With regard to temperature, the $\theta\ vs\ \sqrt{\varepsilon_b}$ relationship was most similar at temperatures between 10° C and 37° C and at temperatures 55° C and 70° C (Fig. 3.5B). This also coincides with the $RMSE$ of the five temperature groups from Eq. 4, which increased greatly above 37° C (Fig. 3.6). The mean $RMSE$ from Eq. 4 at and below 37° C was 0.04 cm^3/cm^3, while above 37° C it was 0.08 cm^3/cm^3 (data not shown). Overall, the measurements made at temperatures 24° C and 37° C were the most

alike in terms of their 95% Cr. I. for the contrasted parameter values, potentially indicating that temperature may not need to be included as a covariate if measurements of $\sqrt{\varepsilon_b}$ are taken between 24° C and 37° C (Fig. 3.5B). However, it is common for the temperature to exceed 37° C within woodchip stockpiles, especially towards the insulated center of large piles where metabolic processes are constantly producing heat (Li *et al.*, 2006). Temperature conditions within agricultural denitrifying beds are typically less than 24° C (Addy *et al.*, 2016).

The specific surface area of a material varies with particle size and controls how much water can be adsorbed, which in turn affects the $\theta\ vs\ \sqrt{\varepsilon_b}$ relationship at varying temperature conditions (Or and Wraith, 1990; Jones and Or, 2002]. Adsorbed water molecules that are 'bound' by intermolecular forces to hydroxyl groups in the cell wall of the woodchip materials are rotationally hindered, which results in a lower dielectric signature (ε_{bw} ~ 5) than 'free' liquid water molecules (Torgovnikov, 1993; Jones and Or, 2002). As a consequence, at low water contents and low temperature, bound water will reduce measurements of $\sqrt{\varepsilon_b}$ through what is known as the 'thermodielectric' effect (Or and Wraith, 1990; Jones and Or, 2002). Conversely, as temperature increases, bound water desorbs and values of $\sqrt{\varepsilon_b}$ tend to increase without change in θ. This phenomenon was most apparent at low water content in the fine woodchip particles (Fig. 3.6A), which have a larger specific surface area than coarse particles (Bekhta and Hazirogl u, 2002). At high water contents, the thermodielectric effect has less influence because all possible sorption sites are occupied, but increases in temperature may noticeably decrease the value of ε_w (*e.g.* values of ε_w at 10° C and 70° C are about 84 and 66, respectively – Or and Wraith (1990)). This effect is slightly apparent in the medium and coarse woodchip mixtures (Fig. 3.6B and C), although the high variability in the measurements and reduced accuracy of the reflectometer at high temperature/water content (Campbell Scientific, Inc., 2016; Kapilaratne and Lu, 2017) makes it difficult to draw any firm conclusions.

3.4.2 Calibration

The $\sqrt{\varepsilon_{sa}}$ of the particular woodchip mixture was subtracted from $\sqrt{\varepsilon_b}$ in Eq. 5 so that the prediction of θ was not influenced by temperature when $\theta = 0\ \mathrm{cm^3/cm^3}$ (Table 3.3). Torgovnikov (1993) reports that solid wood with a similar bulk density to the woodchip materials used in the experiments (0.2 g/cm^3) had $\sqrt{\varepsilon_s}$ values between 1.14-1.18 measured at a TDR frequency of 100-1000 MHz. In this study, values of $\sqrt{\varepsilon_{sa}}$ include the influence of air, and can be used to infer the amount of contact between the woodchips and the waveguides. Values of $\sqrt{\varepsilon_{sa}}$ close to 1 would indicate a prevalence of air voids (*i.e.*, poor contact between the sensor and the solid wood material), whereas $\sqrt{\varepsilon_{sa}}$ values close to $\sqrt{\varepsilon_s}$ would indicate near perfect contact.

Equation 5 with optimized parameter values for fine, medium and coarse woodchip particle sizes fitted the data reasonably well, but $RMSE$ increased with particle size (Table 3.3). Consequently, the 95% Cr.I. and P.I. for the predictions of θ were narrower for the fine in comparison to the medium and coarse woodchip's calibration relationship (Fig. 3.7). This increase may have been caused by poorer contact between the sensor and the woodchips in the coarser mixtures than in fine. This interpretation is reinforced by the fact that one of the fine woodchip replicates had a $\sqrt{\varepsilon_{sa}}$ value (1.13) closest to the dielectric permittivity of solid wood ($\sqrt{\varepsilon_s}$), whereas one of the coarse material replicates had the lowest value of $\sqrt{\varepsilon_{sa}}$ (1.02) (Table 3.3).

The variability in the measurements also increased with temperature (Fig. 3.6). According to the user manual, the CS616-L reflectometers have an operational temperature range from 0° to 70° C, although measurements made at 40° C can have as much as 2% and 6% error when the volumetric water content is 12% and 30%, respectively. Measurement error above 40° C has not been quantified but is expected to be much larger, especially as the woodchips become more saturated (Personal

Communication with Campbell Scientific, Inc.), which is apparent from the scatter of the data points displayed in the 55° and 70° C subplots incorporated in Figure 3.7.

The goodness-of-fit statistics for Eq. 6 were only slightly lower than those for Eq. 5 for the medium and coarse woodchip mixtures (Table 3.3). Application of Eq. 6 is best suited when the particle size distribution for a woodchip mixture is uncharacterized and/or $\sqrt{\varepsilon_{sa}}$ is unknown. Assuming $\sqrt{\varepsilon_{sa}} = 1$ in Eq. 6 is somewhat arbitrary; however, since measurements of $\sqrt{\varepsilon_b}$ should never be less than the dielectric permittivity of air, this value was chosen so that the predicted value for θ could not be negative.

3.4.3 Validation

The d_g (1554 µm) and bulk density (0.296 g/cm^3) of the woodchip mixture used to construct the field pile was determined at the beginning of the experiment and was comparable to the d_g of the 'fine' woodchip mixture used in the calibration (Fig. 3.7) (Kannepalli, 2014). Using the mean parameter values for the fine particle size calibration equation (Table 3.3), the $RMSD$ of the field measured water content was 0.13 cm^3/cm^3 and the bias was 19%. However the validation measurements were taken at the end of the 6-month experimental period, after there was sufficient time for the finer sized woodchip particles to migrate downward towards the bottom of the pile and after the woodchips had undergone decomposition and compaction. When the mean parameter values for Eq. 6 (*i.e.,* "All" in Table 3.3) were used to predict θ, the $RMSD$ was reduced to 0.11 cm^3/cm^3 and the bias was lowered to -10%.

The field validation points that were not contained within the 95% P.I. were located at the bottom edge of the pile (two data points in the 37° C and one in the 55° C subplots of Fig. 3.7), where compaction is purported to be highest and where the finest particles tend to accumulate; and directly in the center (the one data point in the 70° C subplot of Fig. 3.7), where temperature is highest. It should

be noted that the field validation data points were not made exactly at the temperature of the graph they are displayed in, which also could explain some of the variation outside of the temperature-specific P.I displayed in Fig. 3.7.

The laboratory validation measurements were only made at room temperature, but were completed for all particle sizes. These measurements had a $RMSD$ of 0.08 cm^3/cm^3 and a -4% bias using the mean parameter values for Eq. 5 and a $RMSD$ of 0.06 cm^3/cm^3 and a -7% bias using the mean parameter values for Eq. 6 (Table 3.3). The laboratory validation measurement made at a target water content of about 0.6 cm^3/cm^3 in the coarse woodchip mixture had a residual error nearly two times as large as all others from its calibration equation (Fig. 3.7). This is likely a result of the water being preferentially distributed towards the bottom of the container closer to where the waveguides were positioned resulting in an overestimation of θ.

3.5 Conclusions

Measurements of $\theta \ vs \ \sqrt{\varepsilon_b}$ in woodchip mixtures taken with a low-frequency CS616-L water content reflectometer were highly influenced by temperature, and to a lesser extent by particle size distribution. Incomplete contact between the probes and material that occurs in mixtures containing large woodchip particles reduces the accuracy of the calibration and poses a potential problem to practitioners. Future measurements of the $\theta \ vs \ \sqrt{\varepsilon_b}$ relationship taken in woodchip mixtures with particle size distributions different than the mixtures used here can be inserted in the same hierarchical Bayesian framework by incorporating the information contained in the posterior distribution for the parameters provided in this paper (Table 3.3) as prior information for future inferences. The calibration functions provided in this study are best suited for taking measurements in partially saturated woodchips at low (10° C) to moderate (37° C) temperature conditions, like those found in agricultural denitrifying beds (Addy *et al.*, 2016) and towards the periphery of outdoor stockpiles (Kannepalli 2014).

3.6 References

Addy, K., Gold, A.J., Christianson, L.E., David, M.B., Schipper, L.A., Ratiagn, N.A., 2016. Denitrifying bioreactors for nitrate removal: A meta-analysis. *J. Environ. Qual.* 45(3), 873-881.

Afzal, M.T., Bedane, A.H., Sokhansanj, S., Mahmood, W., 2009. Storage of comminuted and uncomminuted forest biomass and its effect on fuel quality. *BioResour. 5*(1), 55-69.

Ansoult, M., Backer, L.W., Declercq, M., 1985. Statistical Relationship between Apparent Dielectric Constant and Water Content in Porous Media. *Soil Sci. Soc. Am. J. 49*(1), 47-50.

Baker, J.M., Lascano, R.J., 1989. The Spatial Sensitivity of Time-Domain Reflectometry. *Soil Sci. 147*(5), 378-384.

Bekhta, P., Haziroglu, S., 2002. Theoretical approach on specific surface area of wood particles. *For. Prod. J. 52*(4), 72-76.

Campbell, G.S., Anderson, R.Y. 1998. Evaluation of simple transmission line oscillators for soil moisture measurement. *Comp. Electron. Agri. 20*(1), 31-44.

Campbell Scientific, Inc., 2016. CS616 and CS625 water content reflectometers instruction manual, Campbell Scientific, Inc., Logan, UT.

Constantz, J., Murphy, F., 1990. Monitoring moisture storage in trees using time domain reflectometry. *J. Hydrol. 119*(1-4), 31-42.

Dahlen, J., Antony, F., Li, A., Love-Myers, K., Schimleck, L., Schilling, E.B., 2015. Time-domain reflectometry for the prediction of loblolly pine and sweetgum moisture content. *BioResour.* 10(3), 4947-4960.

Fenton, O., Healy, M.G., Brennan, F., Jahangir, M.M.R., Lanigan, G.J., Richards, K.G., Thornton, S.F., Ibrahim, T.G., 2014. Permeable reactive interceptors: Blocking diffuse nutrient and greenhouse gas losses in key areas of the farming landscape. *J. Agricult. Sci.* 152(S1), 71-81.

Ferré, P.A., Rudolph, D.L., Kachanoski, R.G., 1996. Spatial Averaging of Water Content by Time Domain Reflectometry: Implications for Twin Rod Probes with and without Dielectric Coatings. *Water Resour. Res. 32*(2), 271-279.

Ferré, T.P., Nissen, H.H., Šimůnek, J., 2002. The Effect of the Spatial Sensitivity of TDR on Inferring Soil Hydraulic Properties from Water Content Measurements Made during the Advance of a Wetting Front. *Vadose Zone J. 1*(2), 281-288.

Gelman, A., Rubin, D.B., 1992. Inference from iterative simulation using multiple sequences. *Stat. Sci. 7*(4), 457-472.

Gelman, A., Hill, J., Yajima, M., 2012. Why we (Usually) don't have to worry about multiple comparisons. *J Res. Educ. Eff. 5*(2), 189-211.

Gelman, A., Carlin, J.B., Stern, H.S., Dunson, D.B., Vehtari, A., Rubin, D.B., 2015. *Bayesian data analysis*, CRC Press, Florida, 3rd ed.

Gelman, A., Hill, J., 2016. *Data analysis using regression and multilevel / hierarchical models*, University Press, Cambridge.

Germann, P.F., 2017. Shape of Time Domain Reflectometry Signals during the Passing of Wetting Fronts. *Vadose Zone J. 16*(2), 1-5.

Gray, A.N., Spies, T.A., 1995. Water content measurement in forest soils and decayed wood using time domain reflectometry. *Can. J. For. Res. 25*(3), 376-385.

Hedmark, A., Scholz, M., 2008. Review of environmental effects and treatment of runoff from storage and handling of wood. *Bioresour. Technol.* 99(14), 5997-6009.

Hernández-Santana, V., Martínez-Fernández, J., 2008. TDR measurement of stem and soil water content in two Mediterranean oak species. *Hydrol. Sci. J. 53*(4), 921-931.

Jitka, M., Zuzana, B., Karel, H., Kateřina, S., Michal, K., Michal, Š., 2017. Sustainability of denitrifying bioreactors with various fill media. *Plant Soil Environ.* 63(10), 442-448.

Jones, S.B., Or, D., 2002. Surface area, geometrical and configurational effects on permittivity of porous media. *J. Non-Cryst. Solids. 305*(1-3), 247-254.

Jones, S.B., Wraith, J.M., Or, D., 2002. Time domain reflectometry measurement principles and applications. *Hydrol. Process. 16*(1), 141-153.

Kannepalli, S., 2014. Environmental issues in organics recycling: reed bed biosolids reuse and leachate from wood mulch stockpiles, Ph.D. Thesis, Rutgers University, New Brunswick, NJ

Kannepalli, S., Strom, P.F., Krogmann, U., Subroy, V., Giménez, D., Miskewitz, R., 2016. Characterization of wood mulch and leachate/runoff from three wood recycling facilities. *J. Environ. Manage*. 182, 421-428.

Kapiliratne, R.J., Lu, M., 2017.Automated general temperature correction method for dielectric soil moisture sensors. *J. Hydrol.* 551, 203-216.

Kelleners, T.J., Seyfried, M.S., Blonquist, J.M., Bilskie, J., Chandler, D.G., 2005. Improved Interpretation of Water Content Reflectometer Measurements in Soil. *Soil Sci. Soc. Am. J. 69*(6), 1684-1690.

Ledieu, J., Ridder, P. Clerck, P., Dautrebande, S., 1986. A method for measuring soil water moisture by time domain reflectometry. *J. Hydrol.* 88(3-4), 319-328.

Lenz, H., Idler, C., Hartung, E., Pecenka, R., 2015. Open-air storage of fine and coarse wood chips of poplar from short rotation coppice in covered piles. *Biomass Bioenerg*y. 83, 269-277.

Li, X., Koseki, H., Momota, M., 2006. Evaluation of danger from fermentation-induced spontaneous ignition of wood chips. *J. Hazard. Mater. 135*(1-3), 15-20.

Lin, Y., Pan, F., 2015. Monitoring Woody Biomass Chips Quality Change during Field Storage in Michigan. *For. Prod. J. 65*(7-8), 327-336.

Logsdon, S.D., 2009. CS616 Calibration: Field versus Laboratory. *Soil Sci. Soc. Am. J. 73*(1), 1-6.

Malicki, M.A., Kotlinski, J. , 1998. Dielectric determination of moisture of wood using time domain reflectometry. *Int. Agrophys.* 12, 217-220.

Malicki, M., Plagge, R., Roth, C., 1996. Improving the calibration of dielectric TDR soil moisture determination taking into account the solid soil. *Eur. J. Soil Sci. 47*(3), 357-366.

Mendel, T., Überreiter, A., Kuptz, D., Hartmann, H., 2016. Comparison of Rapid Moisture Content Determination Methods for Wood Chips. *24th EUBCE*. doi:10.5071/24thEUBCE2016-2BV.1.5.

Nadler, A., Raveh, E., Yermiyahu, U., Green, S.R., 2003. Evaluation of TDR Use to Monitor Water Content in Stem of Lemon Trees and Soil and Their Response to Water Stress. *Soil Sci. Soc. Am. J. 67*(2), 437-448.

Or, D., Wraith, J.M., 1990. Temperature effects on soil bulk dielectric permittivity measured by time domain reflectometry: A physical model. *Water Resour. Res. 35*(2), 371-383.

Paz, A., 2006. Influence of Temperature in Radio Frequency Measurements of Moisture Content in Biofuel. *IEE IMTC P*. doi:10.1109/imtc.2006.235960.

Paz, A., Thorin, E., Topp, C., 2010. Dielectric mixing models for water content determination in woody biomass. *Wood Sci. Technol. 45*(2), 249-259.

Pichler, V., Homolák, M., Skierucha, W., Pichlerová, M., Ramírez, D., Gregor, J., Jaloviar, P., 2011. Variability of moisture in coarse woody debris from several ecologically important tree species of the Temperate Zone of Europe. *Ecohydrol. 5*(4), 424-434.

Plummer, M., Best, N., Cowles, K. Vines, K., 2006. CODA: convergence diagnosis and output analysis for MCMC. *R News*. 6(1), 7-11.

Plummer, M., 2016. rjags: Bayesian Graphical Models using MCMC. R package version 4-6 https://CRAN.R-project.org/package=rjags

Previati, M., Canone, D., Bevilacqua, I., Boetto, G., Pognant, D., Ferraris, S., 2012. Evaluation of wood degradation for timber check dams using time domain reflectometry water content measurements. *Ecol. Eng. 44*, 259-268.

Quinones, H., Ruelle, P., Nemeth, I., 2003. Comparison of three calibration procedures for TDR soil moisture sensors. *Irrig. Drain. 52*(3), 203-217.

Roth, K., Schulin, R., Flühler, H., Attinger, W., 1990. Calibration of time domain reflectometry for water content measurement using a composite dielectric approach. *Water Resour. Res. 26*(10), 2267-2273.

Schimleck, L., Love-Myers, K., Sanders, J., Raybon, H., Daniels, R., Mahon, J., Andrews, E., Schilling, E., 2011. Measuring the moisture content of green wood using time domain reflectometry. *Forest Prod. J.* 61(6), 428-434.

Schindler, U., Durner, W., von Unold, G., Müller, L., 2010. Evaporation Method for Measuring Unsaturated Hydraulic Properties of Soils: Extending the Measurement Range. *Soil Sci. Soc. Am. J.* 74:1071–1083

Sihvola, A., Kong, J., 1988. Effective permittivity of dielectric mixtures. *IEEE Trans. Geosci. Remote Sens. 26*(4), 420-429.

Skierucha, W., Wilczek, A., Szypłowska, A., Sławiński, C., Lamorski K., 2012. A TDR-Based Soil Moisture Monitoring System with Simultaneous Measurement of Soil Temperature and Electrical Conductivity. *Sens. 12*(10), 13545-13566.

Subroy, V., Giménez, D., Qin, M., Krogmann, U., Strom, P.F., Miskewitz, R.J., 2014. Hydraulic properties of coarsely and finely ground woodchips. *J. Hydrol. 517*, 201-212.

Sparks, J.P., Campbell, G.S., Black, A.R., 2001. Water content, hydraulic conductivity, and ice formation in winter stems of Pinus contorta: A TDR case study. *Oecologia. 127*(4), 468-475.

Tao, W., Hall, K.J., Masbough, A., Frankowski, K., Duff, S.J., 2005. Characterization of leachate from a woodwaste pile. *Water Qual. Res. J. Can.* 40, 476–483.

Topp, G.C., Davis, J.L., Annan, A.P., 1980. Electromagnetic determination of soil water content: Measurements in coaxial transmission lines. *Water Resour. Res. 16*(3), 574-582.

Torgovnikov, G.I., 1993. *Dielectric properties of wood and wood-based materials*. Springer-Verlag, Berlin.

van Driel, P.W., Robertson, W.D., Merkley, C., 2006. Denitrifcation of agricultural drainageusing wood-based reactors. *T. ASABE.* 49(2), 565-573.

Wullschleger, S.D., Hanson, P.J., Todd, D.E., 1996. Measuring stem water content in four deciduous hardwoods with a time-domain reflectometer. *Tree Physiol. 16*(10), 809-815.

Table 3.1. Summary of functions that describe the $\theta\ vs\ \varepsilon_b$ relationship in various wood materials. The I.D. refers to its curve displayed in Figure 3.4.

Model	I.D.	Coefficients	Reference(s)
$\theta = a\varepsilon_b^3 + b\varepsilon_b^2 + c\varepsilon_b + d$	1[A]	$a = 4.30 * 10^{-6}$ $b = -5.20 * 10^{-4}$ $c = 2.92 * 10^{-2}$ $d = -5.30 * 10^{-2}$	Schimleck *et al.* (2011); Previati *et al.* (2012)
	2	$a = 6.67 * 10^{-6}$ $b = -1.06 * 10^{-3}$ $c = 5.86 * 10^{-2}$ $d = -3.19 * 10^{-1}$	Constantz and Murphy (1990)
	3	$a = 5.0 * 10^{-5}$ $b = -4.16 * 10^{-3}$ $c = 1.17 * 10^{-1}$ $d = -4.57 * 10^{-1}$	Hernández-Santana and Martínez-Fernández (2008)
	4	$a = 9.0 * 10^{-5}$ $b = -6.9 * 10^{-3}$ $c = 1.79 * 10^{-1}$ $d = -9.88 * 10^{-1}$	Hernández-Santana and Martínez-Fernández (2008)
$\theta = a\varepsilon_b^2 + b\varepsilon_b + c$	5	$a = -4.93 * 10^{-4}$ $b = 4.66 * 10^{-2}$ $c = -2.51 * 10^{-1}$	Wullschleger *et al.* (1996); Nadler *et al.* (2003)
$\varepsilon_b = (\varepsilon_a^\beta * \theta_a + \varepsilon_s^\beta * \theta_s + \varepsilon_w^\beta * \theta)^{1/\beta}$	6[B]	$\beta = 0.36$ $\theta_s = 0.17$ $\varepsilon_s = 10$ $\varepsilon_w = 80$ $\varepsilon_a = 1$	Paz *et al.* (2010)
$\varepsilon_b = \varepsilon_a + \varepsilon_a \sum_{i=1}^{2} \frac{\frac{\theta_i}{3}\sum_{j=1}^{3} \frac{\varepsilon_i - \varepsilon_a}{\varepsilon_a + D_{i,j}(\varepsilon_i - \varepsilon_a)}}{1 - \frac{\theta_i}{3}\sum_{j=1}^{3} \frac{D_{i,,j}(\varepsilon_i - \varepsilon_a)}{\varepsilon_a + D_{i,j}(\varepsilon_i - \varepsilon_a)}}$	7[C]	$D_w = [0.9, 0.05, 0.05]$ $D_s = [1, 0, 0]$ $\theta_s = 0.17$ $\varepsilon_s = 10$ $\varepsilon_w = 80$ $\varepsilon_a = 1$	Paz *et al.* (2010)
$\theta = a\sqrt{\varepsilon_b} + b$	8	$a = 1.74 * 10^{-1}$ $b = -2.37 * 10^{-1}$	Malicki and Kotlinski (1998)
	9	$a = 9.71 * 10^{-2}$ $b = -1.65 * 10^{-1}$	Malicki and Kotlinski (1998)
	10	$a = 1.72 * 10^{-1}$ $b = -2.79 * 10^{-1}$	Malicki and Kotlinski (1998)
	11	$a = 10.19 * 10^{-2}$ $b = -1.0 * 10^{-1}$	Gray and Spies (1995)

[A] Parameter values are the same as Topp *et al.* (1980)

[B] Power Law Model (Roth *et al.*, 1990)

[C] Maxwell-Garnett Mixing Model (Sihvola and Kong, 1988)

Table 3.2. Means (standard deviations) of the effective volumes (cm^3) for the CS616-L sensors during wetting (Saturating) and gravity-driven drainage (Draining) of mixtures of predominantly fine, medium and coarse particle sizes.

Effective volume	Fine		Medium		Coarse	
Saturating	1287.8	(371.1)	1162.8	(261.4)	879.1	(204.4)
Draining	1384.3	(277.3)	1175.5	(130.1)	1112.9	(125.1)

Table 3.3. Summary of the replicate $\sqrt{\varepsilon_{sa}}$ values for the fine, medium and coarse woodchip mixtures and their parameter's posterior distribution (n=40,000 samples) (Eq. 5) given as the mean (standard deviation). The posterior parameter estimates in "All" were derived after pooling the data from the three particle size groups (Eq. 6). The root mean square error ($RMSE$) was inferred simultaneously with the calibration parameters and the coefficient of determination (R^2) was calculated by evaluating the goodness-of-fit of the 40,000 samples in the posterior distribution.

Particle Size	Calibration Parameters				Goodness-of-fit	
	$\sqrt{\varepsilon_{sa}}$	α	β_1	β_2	RMSE	R^2
Fine	1.054/1.127	0.089 (0.001)	1.052 (0.005)	0.047 (0.002)	0.036 (0.0001)	0.957
Medium	1.088/1.096	0.137 (0.002)	0.733 (0.004)	0.089 (0.004)	0.059 (0.0001)	0.923
Coarse	1.045/1.023	0.179 (0.003)	0.612 (0.003)	0.085 (0.004)	0.060 (0.0006)	0.933
All	1	0.147 (0.001)	0.684 (0.003)	0.088 (0.002)	0.067 (0.0004)	0.904

Fig. 3.1 Particle size distributions for the three types of woodchip samples used in the calibration experiments. The dashed lines represent fits with the functions shown. Modified from Subroy *et al.* (2014).

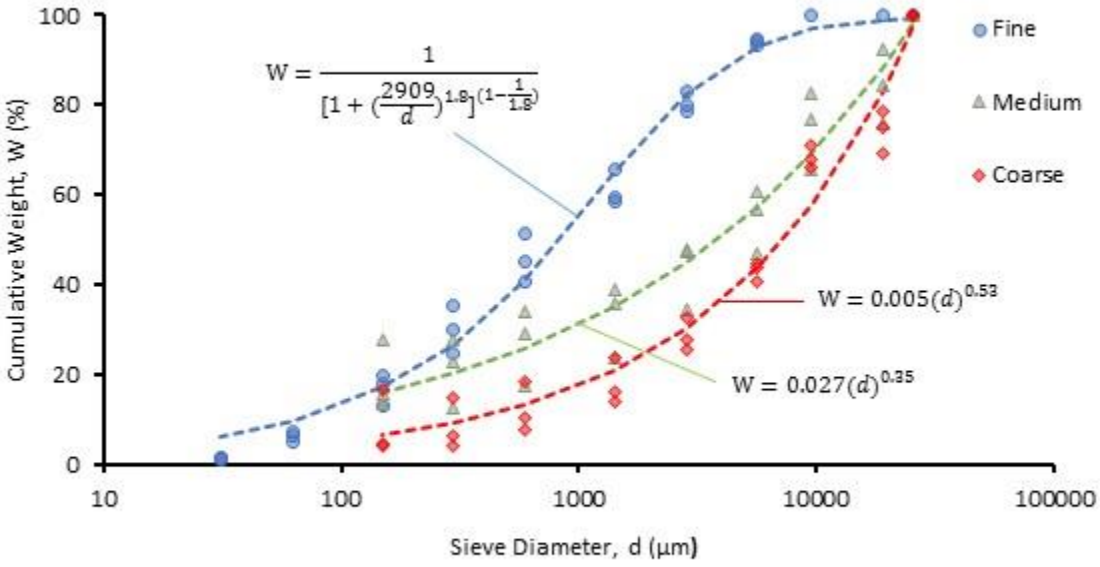

Fig. 3.2 Illustration of the experimental setup. Measurements from the water content reflectometer (CS616-L) and thermistor (109-L) were collected with a data logger (CR1000). Readings from the balances were stored directly in the computer.

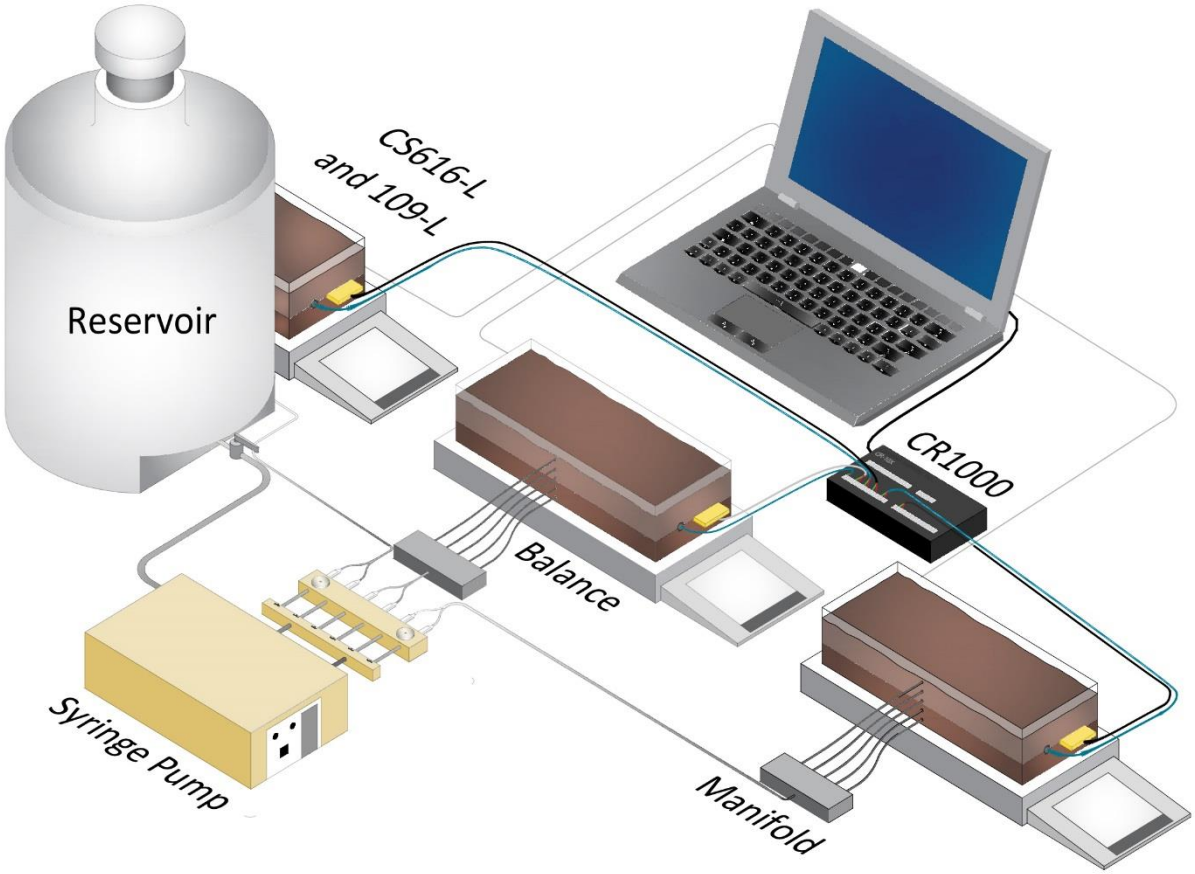

Fig. 3.3 Changes in the output of the CS616-L sensor with respect to the distance of the water level from the waveguide (positioned at Y=0 cm). Measurements were taken while the containers were filled with deionized water and the waveguides were embedded in either the fine mix, coarse mix (Fig. 3.1), or in air. The two-dimensional ellipse (not drawn to scale) depicts the A-A' cross-sectional view of the hypothetical three-dimensional half-ellipsoid effective volume for the coarse woodchip mixture. The three shaded areas represent progressive filling of the container at three times (t) and the associated effect on the sensor's response due to partial filling of the effective volume.

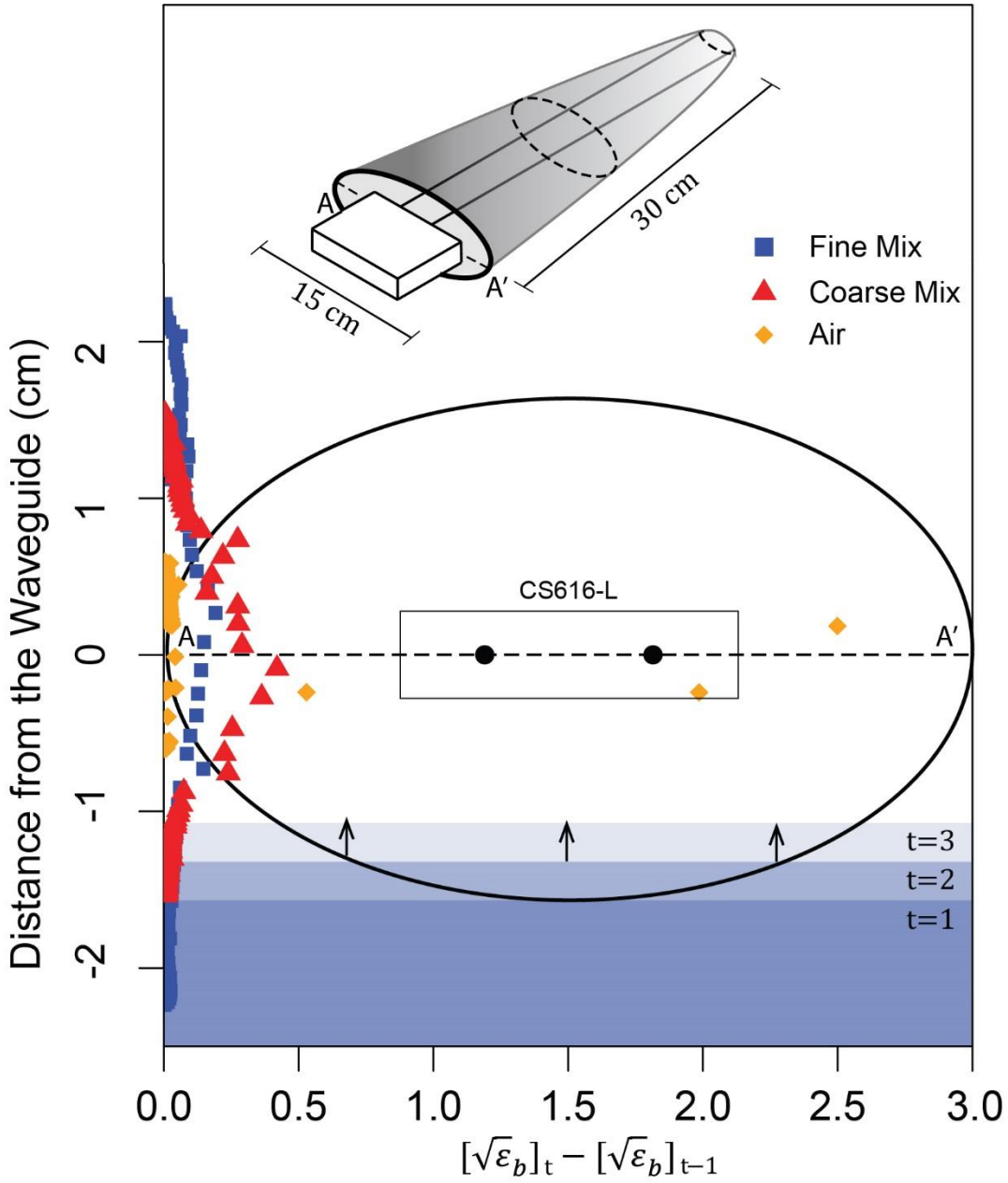

Fig. 3.4 Relationships of A.) θ vs ε_b and B.) θ vs $\sqrt{\varepsilon_b}$ taken from published functions (see Table 3.1) that have been used for various kinds of woody material. The shaded area represents the observed range of measurements made in this study. Each curve spans the θ interval used in its development.

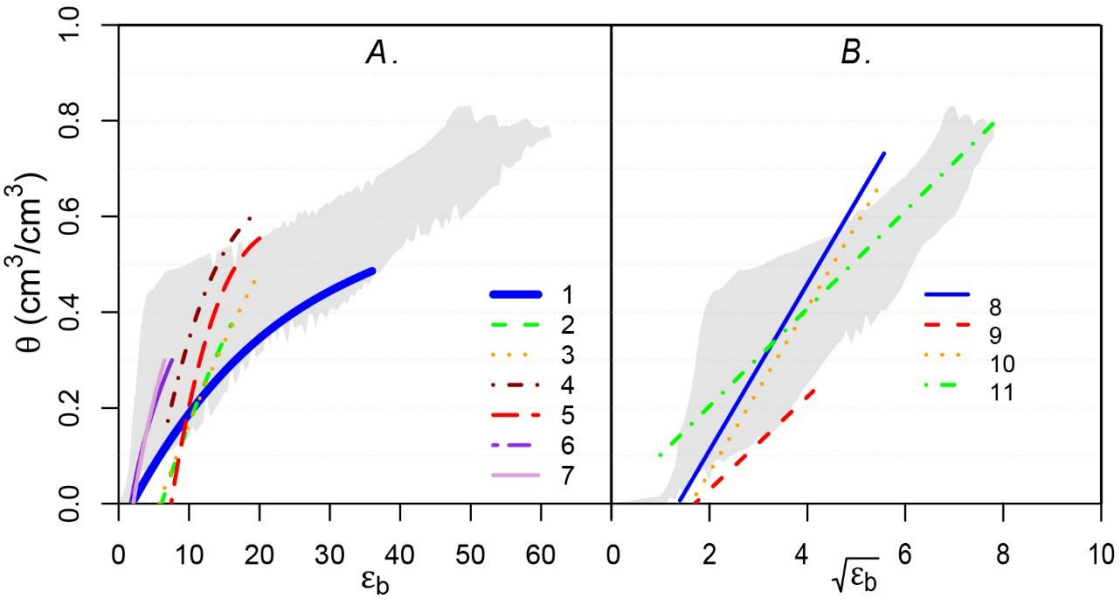

Fig. 3.5 Empirical distributions of the values after contrasting the posterior distributions of the group-level parameters (α, β) of Eq. 4 for A.) particle size and B.) temperature groups. The 95% credible interval for the parameter contrasts are contained within the shaded region of the distribution. The vertical dashed line indicates a contrast equal to 0. Subscripts on the α and β parameters denote which particle size or temperature groups are being compared.

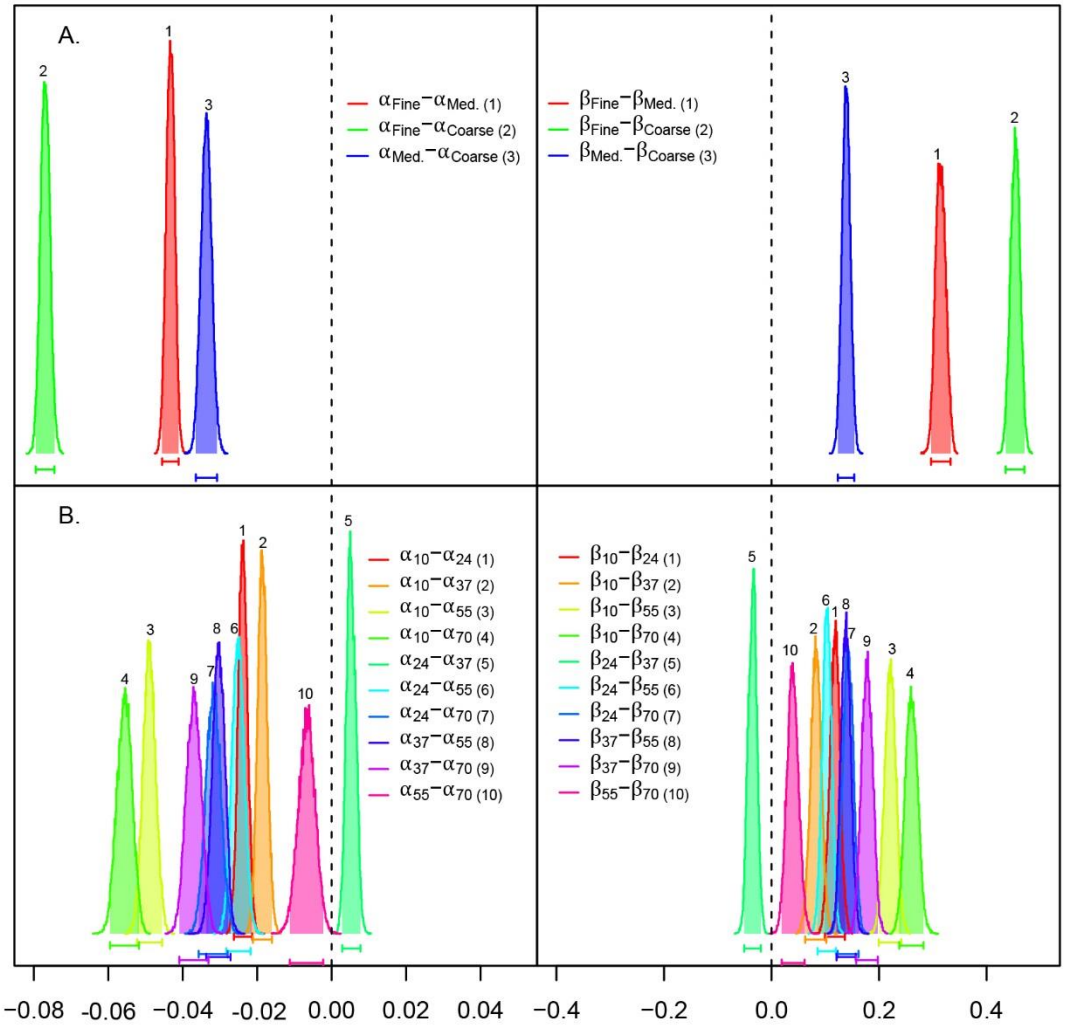

Fig. 3.6 Measurements of $\sqrt{\varepsilon_b}$ for mixtures of predominantly fine, medium and coarse particle sizes made at different temperatures within water content ranges of A.) 0.2-0.25 cm^3/cm^3, B.) 0.4-0.45 cm^3/cm^3 and C.) 0.6-0.65 cm^3/cm^3. The central line represents the median, the ends of the box represent the lower and upper quartiles, the whiskers represent 2.698 standard deviations above and below the median and the symbols are potential outliers.

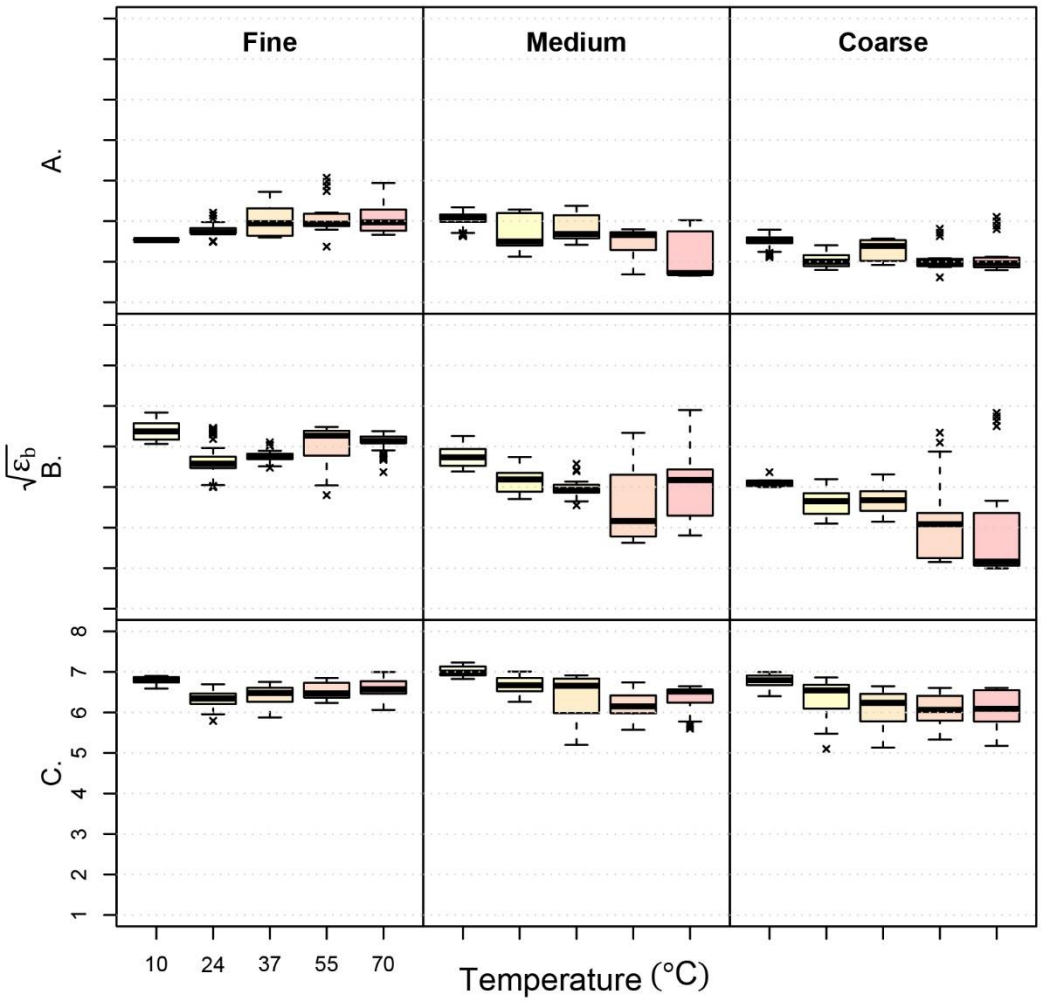

Fig. 3.7 Results of using the posterior distribution for the particle size-specific parameters of Eq. 5 (see Table 3.3). The data are measurements from saturating/draining laboratory experiments (Lab S/D), laboratory validation measurements determined with the gravimetric method (Lab Static) and the field validation measurements from the experimental stockpile (Field). The 95% P.I. interval for θ (*i.e.,* calculated from the posterior estimates of the $RMSE$) is represented by the wider band and the 95% Cr.I. for θ (*i.e.,* calculated from the posterior estimates of the inferred parameters) is represented by the narrower band.

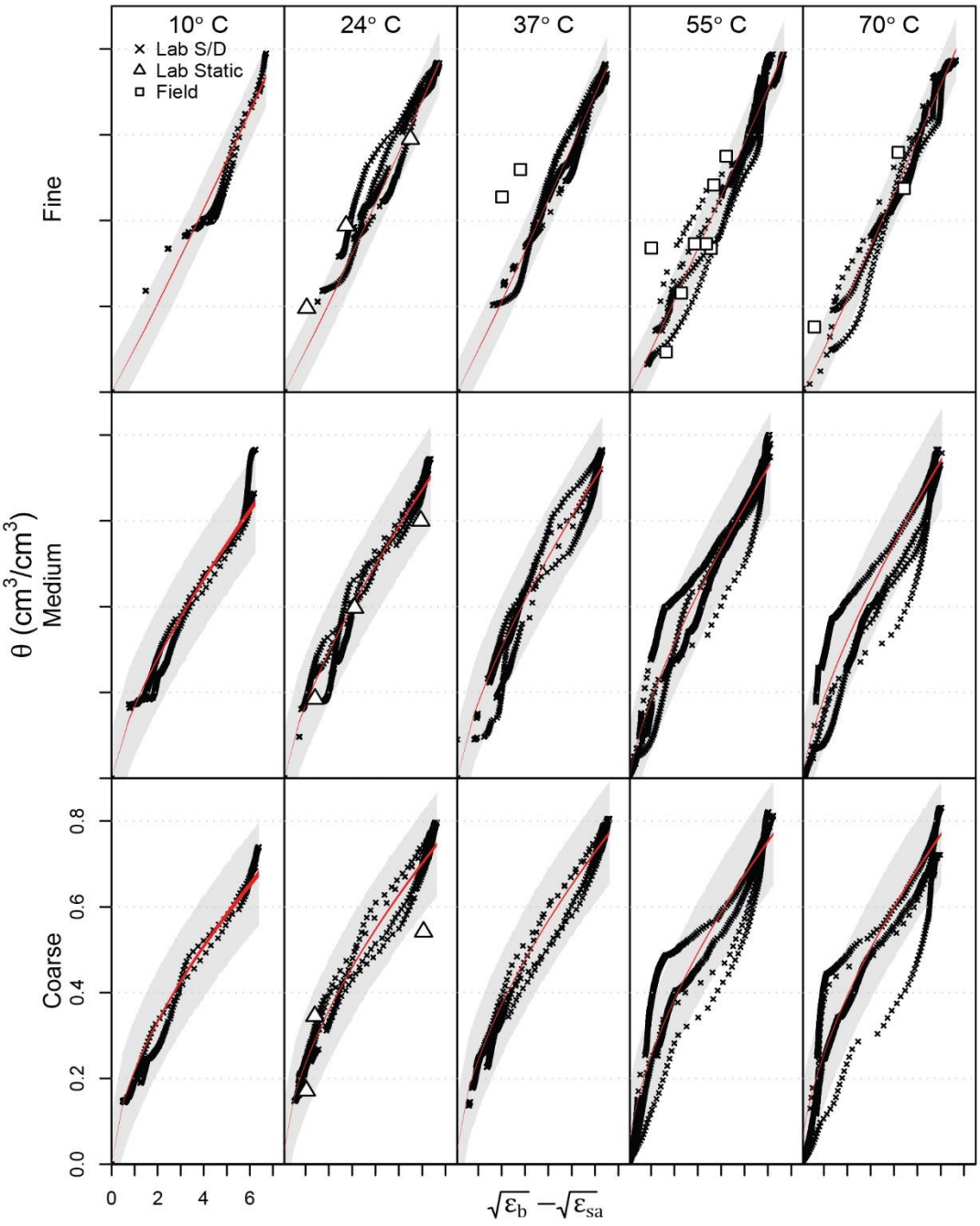

4. Future Work

Coupling the abilities to measure water content and simulate unsaturated flow in woodchips, future efforts of research should be more focused on the dynamics inside the woodchip piles to better understand mechanisms for pollutant transport. With this kind of approach it would be useful to determine the average hydraulic residence time distribution of different piles of woodchips, as this parameter is hypothesized to have a major influence on the quality of the leachate that is generated.

Another important area of research is comparing how the three-dimensional configuration of the woodchip pile influences the quantity and quality of the leachate that is generated. Preliminary investigations (Appendix A) showed that piles configured in a conical shape generated more leachate than windrow-shaped piles. Increasing the surface area to volume ratio of the woodchip piles was also suspected to increase leachate generation. More work is necessary to discover if an optimal woodchip pile configuration exists depending on the goals of management.

Appendices

Appendix A.

Preliminary investigation of how pile size and configuration influences leachate generation during a New Jersey water quality design storm (1.25" of rainfall in 2 hrs at variable intensity). Leachate generation from two types of pile configurations (cone and windrow) and three pile sizes (Small: ~200 m^3; Medium: ~500 m^3; Large: ~1250 m^3) at different initial water contents were simulated in HYDRUS 3D using the optimized parameters (Table 2.4) that describe the hydraulic behavior of fine and coarse woodchip mixtures.

Design Storm Simulations (L)												
Initial Condition	Coarse (ground once)						Fine (ground twice)					
	Cone			Windrow			Cone			Windrow		
	S	M	L	S	M	L	S	M	L	S	M	L
Normal (40%)	10	20	35	0	0	0	5	10	15	0	0	0
Wet (50%)	250	500	1200	400	900	1100	175	400	1100	275	850	1050
Very Wet (60%)	1200	2250	4500	1700	3500	7500	900	1800	4000	1400	3200	7000
Total Rain Volume	3200	5800	10200	4100	7300	14000	3200	5800	10200	4100	7300	14000